PCCP

PERSPECTIVE

View Article Online
View Journal | View Issue

Cite this: *Phys. Chem. Chem. Phys.*, 2025, **27**, 17130

Magneto-chemistry of catalysts for liquid hydrogen production and storage

Ernest Ilisca [ab]

A body of accumulated knowledge on the magneto-chemistry of catalysts for the hydrogen ortho–para conversion is reviewed in order to bridge the gap between theoretical work, laboratory experiments and current industrial needs. Some key issues raised by the conversion of hydrogen nuclear spin isomers, such as its magnetic patterns, which are only partially resolved, are first summarized and the industrial challenges currently faced regarding hydrogen liquefaction and storage are discussed. The theoretical analysis required to understand the quantum characteristics of hydrogen molecules begins with the thermodynamic properties of non-equilibrium mixtures of their two varieties, ortho and para. This is followed by a description of the various electro-magnetic catalytic channels linked to the specific properties of the catalysts, and a study of the energy and momenta exchanges between the catalysts and hydrogen gas. The third section is devoted to the magnetochemistry of catalysts, their morphologies, surfaces and porous structures, their ability to diffuse or adsorb a flow of hydrogen, and measurements of catalytic rates, with particular emphasis on "*in situ*" and "site-specific" experimental methods. The fourth section presents current industrial challenges, highlighting the importance of catalytic steps, and their modeling, in hydrogen liquefaction and storage. The irreversible nature of hydrogen flow through porous catalysts in liquefiers is discussed, and an original short-term hydrogen reservoir model is presented. It is based on the cryogenic, cybernetic, hydrodynamic and catalytic properties of a barrage system of successive microporous catalysts. Finally, break-even times for storage processes are introduced and discussed.

Received 1st April 2025,
Accepted 1st July 2025

DOI: 10.1039/d5cp01260k

rsc.li/pccp

A century of study and research into methods of converting hydrogen from one variety to another is still not enough to understand and master this process. The aim of this review is to bring together the diverse knowledge accumulated on the catalyzed ortho–para conversion, in an attempt to bridge the gap between theoretical work, laboratory experiments and current industrial needs. The difficulty of this project arises from the multiplicity and diversity of disciplines involved in the accomplishment of this catalysis: the quantum structure of the molecule, the magnetism of surfaces, the chemical preparation of catalysts, the thermodynamics of irreversible processes at work in the reaction, the molecular adsorption and electro-magnetic interactions at catalyst surfaces, and the infrared measurement methods and various nuclear spectroscopies.

In the first section, I'll review the various mysteries that have arisen in the ortho–para conversion phenomena, some of which have yet to be solved. This is followed by a selected report on the industrial challenges currently faced in the liquefaction of hydrogen, and then in its storage, in order to promote a decarbonized energy. In the second part, I summarize the theoretical knowledge acquired on conversion mechanisms, their thermal implications and catalytic processes. The third section is devoted to the catalysts, their contact with a hydrogen stream, the reaction channels and their measurements. The fourth section is devoted to the current difficulties facing industrial liquefaction and short-term hydrogen storage, in order to model the use of catalysts. Finally, in the conclusion, I will attempt to draw together the information acquired to discuss the future direction of conversion research.

1. From the molecular hydrogen quantum structure to its energy applications

The intertwining of quantum, spectroscopic and thermodynamical properties of hydrogen molecules led to the 1927 discovery that the proton is a fermion with spin $\frac{1}{2}$. This unified the nuclear spin alternation of the Lyman bands with the differences in the specific heat by considering the gases with odd and even rotational quantum numbers as two separate gases which do not interconvert, the ortho and para varieties.[1] Table 1

[a] *Storage of Hyperfine Hydrogen for Transport, SHYT, F-75013 Paris, France. E-mail: ernest.ilisca@gmail.com*
[b] *Université de Paris-Cité, 10 Rue A. Domon et L. Duquet, 75205 PARIS 13, France*

Table 1 Historical background

1925	Electron spin	G. E. Uhlenbeck and S. A. Goudsmit
1925	Symmetry principle	Wolfgang Pauli
1926	Fermi–Dirac statistics	Dirac–Heisenberg–Pauli–Fermi
1927	Proton spin 1/2	David M. Dennison
1929	Ortho–para H_2	Bonhoeffer–Harteck, Eucken–Hiller
1933	Magnetic conversion	E. P. Wigner

summarizes the foundation of quantum physics in the 1920s structuring the ortho and para states of the hydrogen molecule on the new basis of a symmetry principle.

Their lifetimes are longer than the age of the universe for isolated molecules but are observed to be quite short when the hydrogen interacts with a solid. Their orders of magnitude range from seconds when interacting with magnetic solids, to minutes for noble metals and dielectric oxides, hours for semiconductors, or days for insulating nanocages. These recently measured lifetimes represent new hyperfine measures of nuclear symmetry breaking in the hydrogen molecular space.

Hydrogen conversion became an industrial challenge because almost all liquefied and stored hydrogen (around 10^{10} kg per year, a major part of which is used for aerospace rockets and engines) has to be converted in order to avoid evaporation losses. Undoubtedly, the subject has been dominated for a long time by industrial concerns. The need to feed combustion motors to propel American rockets led to the production and liquefaction of huge quantities of hydrogen. Today, hydrogen is the subject of a great deal of research as a sustainable energy carrier with significant environmental potential. Manufacturers are trying to improve liquefier efficiency by introducing catalysts inside heat exchangers in order to promote continuous conversion down to the lowest temperature (20.3 K).

1.1 Hydrogen mysteries

The quantum structure of hydrogen, linking its electronic and nuclear states, has given rise to many questions and controversies, some of which remain unresolved. Theoretical research remains limited or poorly recognized; the wide variety of disciplines involved complicates the synthesis and the remaining questions are treated as mysteries. The distinction between its nuclear spin isomers, often referred to as different varieties of hydrogen (ortho and para), presents observable macroscopic properties and the property of transforming one variety into the other, hydrogen conversion, remains a subject of research that is all the more active as its energy stakes have become strategic and of industrial concern.

The first mysterious question, linked to the specific thermal behavior of this gas, arose from its division into two distinct varieties characterized by different rotations and different nuclear spin couplings. It was in 1927 that Dennison demonstrated in his ''Note on the Specific Heat of the Hydrogen Molecule'' that the para/ortho ratio of 1/3 at high (~ambient) temperature proved that the proton is a fermion with spin $\frac{1}{2}$.[2] It was not until 1933 that E. P. Wigner interpreted the o–p conversion by paramagnetic molecules. His interpretation is based on the inhomogeneity of the magnetic field created by a magnetic moment that decouples the precession of the nuclear spins of the 2 protons.[3]

20 years later, this theory was extended and enriched by its application to the surfaces of paramagnetic solids on which hydrogen can adsorb and be converted. The sixties were then devoted to the search for the most active paramagnetic catalysts, driven by the aerospace industry. Interested readers can follow the developments in experimental measurements that led to the selection of 3d transition metal oxides (and hydroxides), and in particular the industrial adoption of the ferric oxide catalyst.[4,5] However, the ferromagnetic characteristic of that catalyst, and similar ones, highlighted by Weitzel and his team at the US National Bureau of Standards, remains partially mysterious to this day. Indeed, how can a ferromagnetic surface, producing a particularly homogeneous magnetic field, decouple the spins of 2 protons located at around 0.74 Å from each other? In the dipolar mechanism, hydrogen conversion is a function of the magnetic field gradient produced by the catalyst surface. Regular and ordered arrays of magnetic moments produce a relatively homogeneous magnetic field (at least much more than localized magnetic moments). Experimentally, ferromagnetic catalysts (iron, nickel, *etc.*) are known to induce slow conversion and the inhomogeneity of the surface spin density is recognized to be an important factor for efficient o–p H_2 conversion.

Since 1962, extensive studies of magnetic catalysts were performed by the Californian team of Pr. P. W. Selwood.[6–8] First on alumina-supported oxides, and taking the rate observed on commercial chromia–alumina as a reference, supported 0.5% NiO, 0.5% Ni, and 5% Ni were respectively 5, 53, and 90 times more effective. Puzzled by the contradictory effects of exchange interactions in the catalysts, the authors asked: ''Is there any reason why the presence of ferromagnetism should be associated with catalytic activity?'' but concluded, despite their troubling results, that these observations ''are attributed to accidental factors not related to ferromagnetism''. However, Selwood extensively reported conversion measurements on magnetically concentrated catalysts from 1969. The most remarkable results concern antiferromagnetic samples. The o–p conversion rate on chromia displayed, as a function of temperature, an abrupt change at a Néel transition temperature of 308 K, a pattern representative of the famous ''Hedvall'' effect.[9]

One mystery then followed another. While performing ortho–para (o–p) conversion experiments on such catalysts, Misono and Selwood (MS)[9–11] discovered in 1968 the sensitivity of the conversion rates to the application of an external and homogeneous magnetic field, H. The conversion was accelerated and the rate was found to increase linearly with H at low field values ($H < 1$ kG) and saturate at moderately high field values ($H > 5$ kG). At saturation, the field-induced acceleration could reach 75% for magnetically diluted chromia catalysts. In 1976, similar results were obtained on cobalt and manganese oxides.[11] On CoO, the acceleration was found to be slightly negative at low field ($H < 4$ kG) and then increased without reaching saturation, up to 20% at $H \cong 20$ kG. On MnO, the acceleration was positive and much faster (200% at

$H \cong 20$ kG and not completely saturated). The magnetic field "mystery" is even greater for rare earth catalysts. The catalytic rate was measured to decrease under the influence of a low magnetic field, on a series of rare earths, either self-supported or dispersed on an alumina support.[12] The typical pattern represents a convex decrease below 10 Oe and a concave saturation around 40 Oe, reaching 30 to 40% depending on samples. Even the conversion sensitivity to the Earth's magnetic field was detected! And Selwood commented: "a reexamination might be warranted of the possible role of terrestrial magnetism in the navigation instincts of birds...".[13]

Surprisingly, a new mystery appeared in 1982: a new o–p conversion was observed on non-magnetic noble metals, separately at IBM for silver samples[14] and at Chalmers for copper samples,[15] and later on graphite.[16] Such observations performed by EELS (low energy electron spectroscopy) were very challenging since the o–p transition was supposed to be strongly forbidden in the absence of a nearby magnetic moment (as it requires a simultaneous parity change of the nuclear rotational and spin momenta). Although the EELS experiments could not measure precise conversion rates, they established the primary observation of conversion on (i) non-magnetic catalysts, (ii) metals without chemisorption and (iii) single crystals covered with freely rotating hydrogen molecules. It opened a new branch in the history of hydrogen conversion: the non-magnetic physical catalysis of molecular hydrogen.

From the early 2000s, the non-magnetic conversion "mystery" was observed in numerous insulating catalysts in silicon semiconductors,[17–19] in metal organic framework 74[20] and in amorphous solid water.[21,22] My interpretation of these astonishing measurements will be described in the following theoretical section (Section 2).

The multiplication of unexpected phenomena not only raises fruitful questions, but also provides an unfortunate opportunity to draw attention to work that might otherwise go unnoticed. For instance, the article with the provocative title: "Para–ortho hydrogen conversion: Solving a 90-year old mystery" brings no new information.[23] The paper's conclusion that magnetic dipolar interaction is preponderant in the ortho–para conversion of hydrogen in gaseous media has been known since 1933 and has never been questioned! Nevertheless, it was reinforced by a strange comment made by the editor: "A paramount problem solved at last"!![24]

1.2 Industrial challenges

Between 1954 and 1959, the US National Bureau of Standards laboratories carried out extensive programs to establish the best conversion catalysts. The commercial, military and aerospace interests were to supply the rocket engine testing programs and the hydrogen-fueled rocket vehicles being developed by the Air Force and by NASA, selecting commercial ortho–para converters for their efficient performances in hydrogen conversion.[25] These converters comprise 3d transition metal powdered magnetic oxides (iron, chromium, or nickel) diluted, impregnated, or dispersed inside the selected porous frameworks.[26–28] Various transition metallic oxides such as manganese oxide, ferric oxide, chromium oxide and others in the form of powders or beds were studied. The unsupported hydrous iron oxides proved to be the most effective. Weitzel indicated the formula $Fe(OH)_3$, but it must be stated that no chemical substance with this formula is listed in magnetochemistry reference books, and the exact compound mixtures of the most effective catalysts remained confidential for a long time. Today the commercial unsupported catalyst IONEX is denoted as ferric oxide gel with an (approximate?) formula of Fe_2O_3 and is obtained by gel precipitation. Experimental research is still directed towards the pretreatment of efficient catalysts, interacting with the largest number of molecules and thus composed of porous structures and irregular surfaces dispersing important amounts of magnetic impurities. Catalyst development still requires an empirical approach that combines numerous experimental recipes for surface cleaning and degassing with little rational consideration of building a desired electronic surface structure.

The use of conversion kinetic models in hydrogen liquefaction designs condenses in one observable mean value, the catalytic rate, the resulting effect of many physical phenomena: diffusion through porous structures, adsorption, electromagnetic interactions, and momenta and energy exchanges with the catalyst.[28] The present tendency is to insert the catalyst in the plate-fin thermal exchangers that accommodate direct (and recycling counter) currents; however adjusting the space velocity of hydrogen through the porous structure faces contradictory effects. In particular, enhancing the catalytic rate makes it difficult to evacuate the thermal heat released by the conversion, a challenge at low temperature. The continuous ortho-to-para conversion in commercial hydrogen plants is now promoted by catalyst-filled PFHXs, since the reversible process requires less additional work.[29] However, Mendoza *et al.* demonstrated that the increase in para content is costly in terms of avoiding evaporation losses[30] and argued that partial conversion might be enough for the practical use of hydrogen energy as was already demonstrated by Baker and Shaner of the "Linde" corporation in 1978.[31]

Another industrial challenge concerns the integration of the production of liquid hydrogen with its storage. Important differences appear between the different types of hydrogen storage depending on whether they are intended for short, intermediate or long-term use. In industrial LH_2 applications, short term storage corresponds to daily delivery rates, for instance for a truck delivery or a taxi cab or an airplane daily duty; intermediate storage would be for a week such as in case of sea shipping, while long term storage over several months would correspond to huge reservoirs for chemical industries. The best cryo-compressed vessels can store LH_2 for a week or so before excessive pressure leads to evaporation losses. The best vessels based on adsorption are, to date, unable to permanently retain hydrogen molecules inside the powders and must be complemented by strong containment to sustain high pressures. Chemical adsorption or dilution would retain hydrogen for longer periods; however such metallic surfaces are difficult to desorb.

Nearly all LH_2 storage vessels use metallic double-walled containers that are evacuated and contain multiple layers of alternating metallic and thermally insulated polymeric or glass films to reduce heat leakage into the cryogenic fluid *via* convection, conduction and radiation. These storage vessels are heavy, bulky and expensive implying important investments in their manufacture, production and maintenance costs. Alternatively, I suggested a multiple-walled structure in which microporous plugs would be inserted to regulate the hydrogen flow.[32] Such a barrage-system would delay the pressure and temperature increases through successive *J–T* expansions and catalyzed conversion. The concept of dormancy, introduced in hydrogen storage technologies, relates the energy absorption capacity of a vessel to the rate of heat transfer from the environment. A better correlation of the end use of the stored energy with the duration of each particular transport would enable liquid hydrogen production to be adjusted to its current demand.

2. Hydrogen spin isomers: theoretical concepts

This section, devoted to the theoretical analysis of conversion, begins with a paragraph describing the thermodynamic properties of an arbitrary mixture of the ortho and para varieties of hydrogen. This reminder requires a recapitulation of the formulas for the main thermodynamic potentials, as most analyses consider mixtures in equilibrium with a thermostat, whereas the phenomena at work in liquefiers relate to non-equilibrium flows of hydrogen. On the other hand, in the following paragraphs devoted to the conceptual analysis of conversion processes, the theoretical interpretation presents the phenomena in relation to experimental observations and measurements, without algebraic formulas (the interested reader is therefore referred to original articles for further details).

2.1 Quantum structure and thermal energies

Hydrogen molecules have the peculiar and rare property of a quantum structure macroscopically observable at room temperature by various spectroscopic or thermal techniques. It is possible to distinguish those molecules which have their proton spins parallel or antiparallel and these modifications are diversely denoted as spin isomers, or spin manifolds or ortho (o) and para (p) varieties.[1,33,34] Hydrogen gas is thus composed of a mixture of these two varieties in a definite ratio when it is equilibrated with a thermostat at a fixed temperature. The ortho (o) and para (p) varieties might be considered as independent gases but only specific proportions are in thermal equilibrium with the environment. For most o–p mixtures in contact with a thermal bath, irreversible processes drive the mixture. These non-equilibrium mixtures are stable for very long periods, during which each variety equilibrates separately with the thermostat but not with each other.

2.1.a Hydrogen molecule spin isomers. The existence of the nuclear spin isomers—ortho (o) and para (p) varieties of molecular hydrogen—illustrates that the Pauli Principle applied to the protons induces a ''spin-rotation'' coupling (the total molecular hydrogen wave function belongs to the alternate representation of the permutation group of the nuclei). In the fundamental $X^1\Sigma_g^+$ state the nuclear spin and rotational states have opposite parities. At room temperature, the non-magnetic ($I = 0$) para manifold (antiparallel nuclear spin configuration) is split in two different rotational components, $J = 0$ and $J = 2$, about 600 cm^{-1} apart. A para H_2 mixture equilibrated at 300 K contains about equal proportions of molecules in the rotational states $J = 0$ and $J = 2$. The ortho manifold is magnetic and characterized by a ''parallel'' nuclear spin configuration. Although the total nuclear spin manifolds, $I = 0$ or 1, result from the angular addition of the two protons' half-integer spins, their energy differences are related to the overall molecular rotation and lie in the far infra-red region. In particular the first two ortho and para states ($J = I = 1$) and ($J = I = 0$) are about 118 cm^{-1} = 14.7 meV apart, as schematically represented in Fig. 1.

2.1.b Molecular populations and energies. Let us first consider a sample of hydrogen in thermal equilibrium with a reservoir at temperature T.[34] The partition function Z_J of any rotational state J with degeneracy g_J and energy ε_J is obtained from the Boltzmann statistical distribution: $Z_J = g_J e^{-\varepsilon_J/kT}$. Each population of the degenerate states J is then given by $n_J(T) = Z_J/Z$, where the total partition function $Z = \sum_J Z_J$.

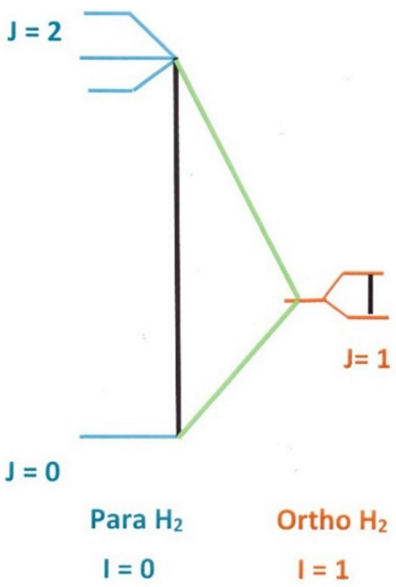

Fig. 1 The nuclear spin-rotation energy levels of the {*I*–*J*} hydrogen system. The nuclear spin triplet ($I = 1$) of the ortho manifold ($J = 1$) is surrounded by a pair of spin singlets ($I = 0$), the para states with lower ($J = 0$) and higher rotational energies ($J = 2$). Ortho states are indexed by their rotational magnetic quantum number, m_J. (The represented nuclear rotational splitting of the ortho ($I = J = 1$) manifold is not scaled and the weak proportion of molecules in the $J = 3$ state of population $\ll 0.09$ is neglected.)

The populations of each manifold, defined by the nuclear spin character, are given by either the total ortho concentration, $o(T) = \sum_{J\ \mathrm{odd}} n_J$, or the para concentration, $p(T) = \sum_{J\ \mathrm{even}} n_J$, taking into account the total concentration satisfying o + p = 1. The rotational space can thus be divided in two manifolds corresponding to the ortho and para varieties $v = \{\mathrm{o}, \mathrm{p}\}$. Their partition functions $Z_v = \{Z_\mathrm{o}, Z_\mathrm{p}\}$ are defined by $Z_v = \sum_{J\in V} Z_J$, the ortho and para populations are given by $v(T) = \dfrac{Z_V(T)}{Z(T)}$, where: $Z(T) = \sum_V Z_V$. The equilibrium ratio, $\rho(T) = \mathrm{o}(T)/\mathrm{p}(T)$, is often used by experimentalists to check if the whole sample has reached thermal equilibrium. More generally, it seems useful to use the ortho–para population ratio as a parameter that characterizes the proportion of the two manifolds $\rho = \mathrm{o/p}$. In most cases each manifold reaches its thermal equilibrium in a time much shorter than the full relaxation time required to equilibrate the mixture.

2.1.b.1 Non-equilibrium mixtures. Non-equilibrium mixtures, defined by their parameter $\rho = \mathrm{o/p}$, can be prepared either by changing the temperature of the thermal bath, or by chromatographic separation, or by mixing two samples with different o/p proportions. The mixtures commonly investigated in the experimental studies are prepared by a thermal method, for example the normal hydrogen n: $\rho(n) = 3 \cong \rho(300\ \mathrm{K})$, the pure para p: $\rho(\mathrm{p}) = 0 \cong \rho(0\ \mathrm{K})$, and the half-half mixture h: $\rho(h) = 1 \cong \rho(77\ \mathrm{K})$. However, mixtures prepared by chromatography might reach larger ortho enrichment, in particular for pure ortho-hydrogen $\rho(\mathrm{o}) \to \infty$.

In the following we introduce the notation $e(T)$ for a hydrogen sample in complete equilibrium with a reservoir at temperature T and $s(\rho, T)$ for an arbitrary hydrogen mixture of ortho and para varieties in separate equilibrium with a reservoir at T. If the mixture is first prepared in a proportion ρ that corresponds to an initial equilibrium at temperature t $\rho(t)$ and then brought into contact with a reservoir at a different temperature T with an unchanged proportion $\rho(t)$, the mixture will be denoted $s(t, T)$.

2.1.b.2 e(T). At global thermal equilibrium T, the relative population of a state J, $n_J(T) = n_J(T) = N_J/N$, is given by the partitions ratio: $n_J(T) = Z_J/Z$. In contact with a thermal reservoir, the manifolds V are equilibrated with one another at T with global populations $v(T) = \dfrac{Z_V(T)}{Z(T)}$, the two varieties being sub-manifolds of the same gas. Each state with population n_J carries the energy $n_J\varepsilon_J$, the energy of each manifold is: $E_V(T) = \sum_{J\in V} n_J(T)\varepsilon_j$. By defining the energy density of variety V as $\varepsilon_V(T) = RT^2\partial_T \ln Z_V(T)$, the energy of each variety as well as the total energy is obtained as:

$$E_V(T) = v(T)\varepsilon_V(T) \tag{1}$$

$$E(T) = \sum_V E_V(T) = \sum_V v(T)\varepsilon_V(T) \tag{2}$$

2.1.b.3 s(ρ, T). When each manifold is equilibrated with a thermostat at T but not one another, the population of a state J belonging to the variety V in the mixture of proportion ρ can be written as $n_{J\in V}(\rho, T) = n(J \in V, \rho, T) = n_J(T)\dfrac{v(\rho)}{v(T)} = v(\rho)\varsigma_J(T)$, where $\varsigma_{J\in V}(T) = \dfrac{n_J(T)}{v(T)} = \dfrac{Z_J}{Z_V}\cdot\varsigma_{J\in V}(T)$ represents the relative population of a state J belonging to a single variety V equilibrated at T satisfying $\sum_{J\in V}\varsigma_J = 1$ and $\sum_{J\in V} n_J(\rho, T) = v(\rho)$. Recall that $v(\rho)$ is either the total ortho concentration $o(\rho) = \sum_{J\ \mathrm{odd}} n_J$ or the para concentration, $p(\rho) = \sum_{J\ \mathrm{even}} n_J$, experimentally prepared at the relative concentration ρ, with populations $v(\rho) = \{\mathrm{p}(\rho), \mathrm{o}(\rho)\}$; in the absence of interconversion, the two manifolds behave as two distinct gases mixed in the proportion ρ. The energy density of variety V remains identical to the equilibrated case $\varepsilon_V(T)$ and the rotational energy of the mixture remains a linear combination of the individual variety energies:

$$E(\rho, T) = \sum_v v(\rho)\varepsilon_V(T) \tag{3}$$

When the mixture ρ prepared at T is brought to equilibrium the energy released, $E(T) - E(\rho, T) = \sum_v \{v(T) - v(\rho)\}\varepsilon_V(T)$, represents the ''Conversion Heat'' of the mixture ρ at T.

2.1.c Irreversibility patterns: specific rotational heat and entropy

2.1.c.1 e(T). At global thermal equilibrium T, the specific heat C of a hydrogen sample at global equilibrium is expressed in terms of the partition function: $C(T) = R\partial_T\{T^2\partial_T \ln Z(T)\}$

2.1.c.2 s(ρ,T). For a hydrogen sample with an arbitrary concentration of spin isomers $v(\rho)$, each variety has its own specific heat (separate equilibria) and the rotational specific heat $C(\rho, T)$ of the mixture is a linear combination of the individual varieties: $C(\rho, T) = \sum_v v(\rho)C_V(T)$, where $C_V(T) = R\partial_T\{T^2\partial_T \ln Z_v(T)\}$. However, as the mixture converges towards equilibrium at T, $\rho \to \rho(T)$, ρ changes continuously, at a certain rate that might depend on the temperature. Thus, the limit reached by $C(\rho, T)$ when $\rho \to \rho(T)$ differs from the equilibrium one:

$$C(T) \neq C(\rho(T), T) = \{\mathrm{o}(T)C_\mathrm{o}(T) + \mathrm{p}(T)C_\mathrm{p}(T)\} \tag{4}$$

Such a discontinuity was first underlined by Dennison who observed that the rotational specific heat of a gas in which the hydrogen o–p equilibrium is momentarily established is completely different from the one in which a mixture is prepared with an unchanged o/p ratio such as the normal one. In general, the specific heat at global equilibrium, $C(T)$, cannot be expressed as a linear combination of the individual specific heat values.

The discontinuity, $\Delta C = C(T) - C(T, T) = R\partial_T\left\{T^2\partial_T \sum_v v(T)\ln v(T)\right\}$, can be related to the irreversible flow and to the entropy creation. It is interesting to underline that the irreversible return to a thermodynamical equilibrium changes

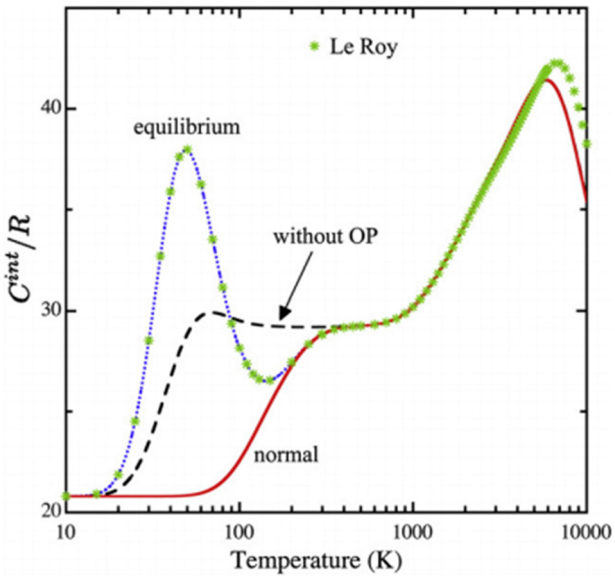

Fig. 2 Molecular hydrogen gas specific heat. The specific heat of an equilibrium mixture of ortho and para varieties (e), compared to the normal one (n), displays a large difference at low temperatures and coincides at higher temperatures.

the o/p proportion and thus the mixing entropy. For example the specific heat of an e-mixture is maximum at low temperature as represented in the Fig. 2 (around T = 50 K, $C \cong 4$ cal mole^{-1}), whereas at that temperature the individual specific heat values are vanishingly small ($C_v(T) \leq 4 \times 10^{-2}$ cal mole^{-1}).

The specific heat of an e-mixture converges towards a linear combination of the individual specific heat values only above 150 K and in particular towards that of the normal mixture. Therefore, the measurements of the o/p proportion at low temperatures based on specific heat values, or on related variables, are questionable.

For similar reasons the rotational entropy of an arbitrary mixture equilibrated separately at T includes a mixing entropy in addition to the entropies of its components $S^r_V(T) = R\partial_T T \ln Z_V(T)$:

$$S(\rho, T) = S^r(\rho, T) + S^c(\rho) \quad (5)$$

$$S^r(\rho, T) = \sum_V v(\rho) S^r_V(T) \quad (6)$$

$$S^c(\rho) = -R \sum_V v(\rho) \ln v(\rho) \quad (7)$$

Note that the expression for the entropy of a totally equilibrated mixture, $S(T) = \partial_T RT \cdot \ln Z(T)$ includes both a combination of the individual entropies as well as the mixing entropy since: $S(\rho(T), T) = R \sum_V v(T)\{\partial_T T \ln Z_V(T) - \ln v(T)\} = \partial_T RT \cdot \ln Z(T) = S(T)$. Therefore, a non-equilibrium hydrogen gas behaves as a mixture of two different gases, whereas an equilibrated one behaves as a single component one.

2.1.d Free energies and availability. The entropy patterns might be analyzed in terms of free energies, which have simpler forms. At global equilibrium, $e(T)$: the expressions for energy and entropy lead to the free energy of an equilibrated mixture: $F(T) = E(T) - TS(T) = -RT \ln Z(T)$.

$s(\rho, T)$: at separate equilibrium, it is worth defining the free energy of an arbitrary mixture:

$F(\rho, T) = E(\rho, T) - T\, S(\rho, T) = \sum_v v(\rho)\{F_V(\rho, T)\}$. It is then possible to deduce the free energy of an arbitrary mixture from the one of a globally equilibrated mixture:

$$F(\rho, T) = F(T) + RT \sum_v v(\rho) \ln \frac{v(\rho)}{v(T)} \quad (8)$$

Summarizing, the expressions of the free energies of the different mixtures have simpler forms than the entropic ones. They might be calculated first and the corresponding entropies can be deduced from them; for equilibrated samples: $S(T) = \frac{\{E(T) - F(T)\}}{T}$, and $S(\rho, T) = \frac{\{E(\rho, T) - F(\rho, T)\}}{T}$ for non-equilibrium mixtures. When heat is exchanged with a thermal bath at T_0 and work delivered or received, it is worth defining at equilibrium the availability:

$$A(T) = E(T) - T_0\, S(T) = E(T)\left\{\frac{T - T_0}{T}\right\} - F(T)\left\{\frac{T_0}{T}\right\} \quad (9)$$

For a mixture prepared in a different proportion, the corresponding availability of each variety has similar forms: $A_V(T) = E_V(T) - T_0 S_V(T)$; and the mixture in separate equilibria obeys similar relationships with the entropy: $A(\rho, T) = \sum_v v(\rho) A_V(T) = E(\rho, T) - T_0\, S^r(\rho, T)$.

Again, the irreversible flow towards global equilibrium is related to the conversion process:

$A(T) - A(\rho, T) = T_0\{S^r(\rho, T) - S(T)\} = -T_0 \Delta S_{conv}(\rho, T)$. At the limit $\rho \to \rho(T)$ the availability variation is related to the mixing entropy:

$$A(T, T) - A(T) = T_0 \Delta S_{conv}(T, T) = T_0 S^c(T) = T_0 S_{mix}(T) = -RT_0 \sum_v v(T) \ln v(T) > 0 \quad (10)$$

Illustration of the non-equilibrium hydrogen gas behavior as a mixture of two different gases will be given in Section 4.1.

2.2 Magnetic conversion processes

For almost a century, hydrogen has been and still is practically converted to thermodynamic proportions by passing through a magnetic catalyst, since only local magnetic gradients were known to be capable of breaking the spin and rotational nuclear selection rules.[33–36] The catalytic process that induces the molecular conversion can be characterized by a simple fundamental and double o–p selection rule: $\Delta J = \Delta I = 1$. In the magnetic mechanism both selection rules are satisfied simultaneously in a single reaction.

2.2.a The dipolar process D. The hydrogen conversion observed by Farkas and Sachsse in oxygenated gaseous mixtures

was interpreted by Wigner in 1933.[3] It relies on the inhomogeneous magnetic field created by the paramagnetic molecule that uncouples the 2 nuclear spins of a scattered hydrogen molecule. The conversion rate is found to be proportional to: $\mu^2 d^{-6}$, with μ being the magnetic moment of the catalytic center and d the (molecule–catalyst center) distance. It was first extended to hydrogen on solid paramagnetic ionic catalysts by Harrisson and McDowell in 1953,[37] but the first microscopic analysis on a catalyst surface was not until 1972.[35] In that model, the magnetic dipoles are assumed to be localized at catalyst ionic centers on the surface and different hydrogen motions such as localized, hopping or diffusing along the surface were considered. The rotational motion was first assumed to be parallel to the surface local plane and later extended to various orientations. The dipolar interaction, being of very short range, requires the molecule to approach very close to the surface electrons and since the 3d ions are relatively concentrated around their center, it is usually assumed that the average interaction is equivalent to that of a molecule with a magnetic moment located at the ionic center and a molecule approaching, let's say less than 3 Å. Note that the magnetic field must be sufficiently inhomogeneous to uncouple the two hydrogen nuclear spins. In particular a homogeneous magnetic field should not affect the conversion.

The amplitude of that dipolar coupling was later compared to the relativistic hyperfine contact as a function of the relative extension and orientation of the electron orbitals of the catalyst ions and of the molecule–ion distance. Evidently, the surface orbitals pointing towards the molecule and having large extensions overlapping with the molecular electron cloud lead to fast conversion rates. The hyperfine contact process was found to overcome the dipolar one at distances shorter than 2 Å but only with appreciable electron overlap;[38] however at such short distances the molecule–ion electronic complex cannot be considered as a simple addition of individual species.

2.2.b Magnetic field effects. The discovery in 1968 of the sensitivity of o–p conversion rates to the application of an external and homogeneous magnetic field H, observed at different concentrations of chromia impurities inserted in alumina,[9–11] was very surprising. The conversion was accelerated and the rate was found to increase linearly with H at low fields ($H < 1$ kG), and saturate at moderately high fields ($H > 5$ kG). At saturation the field acceleration could reach 75% for magnetically diluted chromia catalysts. In 1976, similar results were obtained for cobalt and manganese oxides.[9] On CoO, the acceleration was found to be slightly negative at low fields ($H < 4$ kG) and then increased without reaching saturation, up to 20% at $H \cong 20$ kG. For MnO, the acceleration was positive and much faster (200% at $H \cong 20$ kG and not completely saturated).

These very surprising results remain controversial. First, a homogeneous magnetic field induces simultaneous precession of the nuclear spins, whereas the ortho–para transition needs their dephasing. Second, the magnetic energy μH of the magnetic moments μ remains negligible compared to the ortho–para fundamental energy $\mu H \sim 1\ \mathrm{cm}^{-1} \ll h\omega_{op} \cong 120\ \mathrm{cm}^{-1}$. It is also negligible when compared to thermal energies $\mu H \ll kT$, at experimental temperatures $T > 150$ K and cannot thus affect the nuclear populations. It was recognized in the 1960s that transition metal oxides incorporating dispersed 3d magnetic ions at the surface of a diamagnetic substrate provide efficient catalysts.[6] A typical system, extensively investigated by Selwood consisted of different concentrations of chromia impurities inserted into alumina and these catalysts displayed the magnetic field effects.

I suggested that transitions inside the first order spin–orbit splittings of the catalyst ionic states in the oxide structure could counterbalance the nuclear o–p rotational transition.[39] When the electronic and rotational energy splittings are both on the order of 100 cm^{-1}, a simultaneous transition inside the electron ionic system opposite to an ortho–para one allows the magnetic field to modulate the overall transition energy. However the resonance condition is not always fulfilled. The paradoxical arguments regarding the general lack of reproducibility of the experimental measurements commonly opposed to such a magnetic sensitivity can be simply understood, since the magnetic effects can be observed only in the close vicinity of the resonance. They occur for exacting relationships among the parameters and Misono and Selwood had to try empirically many catalyst pretreatments to sift out the magnetic effects. Consequently, most magnetic effects are not easily reproducible. Inversely, if a magnetic field acceleration is observed experimentally, it seems likely that the catalyst is operating near a molecule–catalyst resonance. The magnetic field accelerations of the conversion remain open to further investigation. A simple test would be to increase the intensity of the applied magnetic field beyond 20 kG. After the conversion rate has reached its maximum the resonance mechanism predicts a subsequent decrease. Since at exact resonance the catalytic rate is sharply enhanced, the magnetic field effects could be used to explore energy transfers between the molecule and catalyst.

No explanations have been proposed until now for the conversion rate decrease measured over rare earth catalysts, under the influence of very low magnetic fields around 40 Oe, reaching 30 to 40% depending on the sample and support, but some spin-rotation level crossings may be suspected.

2.2.c Ferromagnetic conversion. Let me briefly summarize some experimental facts supporting the magnetic enhancement of catalytic activity. Very early on, Weitzel noticed that samples with some degree of ferromagnetism exhibited the highest catalytic activity. Svadlenak and Scott[40] underlined that the catalytic activity on oxide mixtures decreased in the following order: ferromagnetic > antiferromagnetic > paramagnetic. In his study, the alumina-supported ferric oxide showed the highest activity. Selwood reported measurements on magnetically concentrated catalysts, extensively from 1969. The most remarkable results concerned antiferromagnetic samples. Chromia, cobalt monoxide and manganese monoxide were investigated. The o–p conversion rate on chromia displayed, as a function of temperature, an abrupt change at a Néel transition temperature of 308 K.[13]

The abundance of experimental evidence for the ferromagnetic character of Fe, Cr or Ni catalysts has led me to consider

the dynamic behavior of these catalysts. The exchange of angular momentum and energy between molecular rotation and catalyst spin waves enables very rapid conversion. This resonant effect is a manifestation of the catalyst's collective behavior, not a simple surface phenomenon. A simple approach was then to classify the efficiency of catalysts according to their neighbor-to-neighbor exchange integrals. The fastest conversions are not those occurring on strong ferromagnetic catalysts ordered by fields of 10^6 Gauss, but rather on more disordered ones characterized by intermediate fields of 10^5 Gauss.

Magnetic catalysts such as $Fe(OH)_3$, $Cr(OH)_3$, and $Ni(OH)_2$, whose molecular fields are about 100 kG, belong to the category of weak ferromagnets such as ferrimagnetic ones and have a high probability of having a spin-wave in the resonant region $\omega_q = \omega_{op}$. They were thus assumed to belong to the class of magneto-catalysis effectiveness.[42,43] On the other hand, strong ferromagnets such as Fe_3O_4, or pure Ni characterized by optical magnons or paramagnets have a lower probability of exhibiting a spin-wave of high density around the resonance condition. In 2006, measurements of ortho–para H_2 conversion on multiple-decked sandwich clusters of $M(C_6H_6)_2$ (M = Mn, Fe, Co) demonstrated that the inhomogeneity of spin density distribution is an important factor for the best o–p H_2 conversion.[44] Noticing that the spin-wave energy of the chromium spins is on the order of 1–50 meV, they concluded that the 14.7 meV rotational energies of o-H_2 should be possibly dissipated into magnetic degrees of freedom. This suggests that the Cr or Fe ion pairs in the IONEX and Oxisorb catalysts play an important role in the absorption of the o–p energy.

2.3 Electro-magnetic conversion channels

In 1986, S. Sugano and I considered a new channel to interpret the conversion rates of hydrogen on chromia–alumina surfaces.[45] Since Coulomb interactions mix the molecular and catalyst electrons, a surface electron can come in contact with the adsorbed protons through the antibonding molecular orbital. Nuclear perturbations are so weak that even a very small electronic effect might overcome the nuclear disturbance. We denoted this second-order process, schematically illustrated in Fig. 3, as the XY exchange–contact conversion. In a first electronic virtual step, the molecule–solid repulsion excites the molecule and evacuates the H_2 rotation momenta while the hyperfine contact links the excited electrons to the nuclear spins in a second magnetic step. Here a new concept arose in the conversion theory: the hyperfine interaction cannot be reduced to a purely nuclear transition but involves also an electronic one. For the first time, the hydrogen conversion on a magnetic surface was not assumed to be induced by magnetic point dipoles.[45]

2.3.a Metal physical catalysis

2.3.a.1 Noble metals. Strangely, hydrogen conversion was observed to occur on noble metals *via* EELS (electron energy loss spectroscopy) measurements in 1982.[14–16] P. Avouris at IBM labs first reported that the ortho molecules deposited on a surface of silver (111) had probably converted into their para form, before the time of about 10 min necessary to run the apparatus.[14] Similar effects were reported shortly later, on Cu(100)[15] and on graphite.[16] In all cases, the rates were too fast to be registered. These experiments established the primary observation of conversion on non-magnetic catalyst single crystals covered with freely rotating hydrogen molecules. All the existing models relied on catalyst magnetic moments, usually from incomplete shells of transition metal ions: 3d or 4f ones inserted on a substrate. These processes were inefficient for diamagnetic surfaces, since these substrates have full and closed shells and no magnetic moments.

In 1990 I spent a sabbatical year at Osaka University to understand why and how hydrogen undergoes conversion on noble metal surfaces at a rather low temperature of 10–15 K, and why the process is so fast on Ag(111). The first challenge was to understand how a non-magnetic substrate could induce magnetic conversion. I concluded that the only possibility was

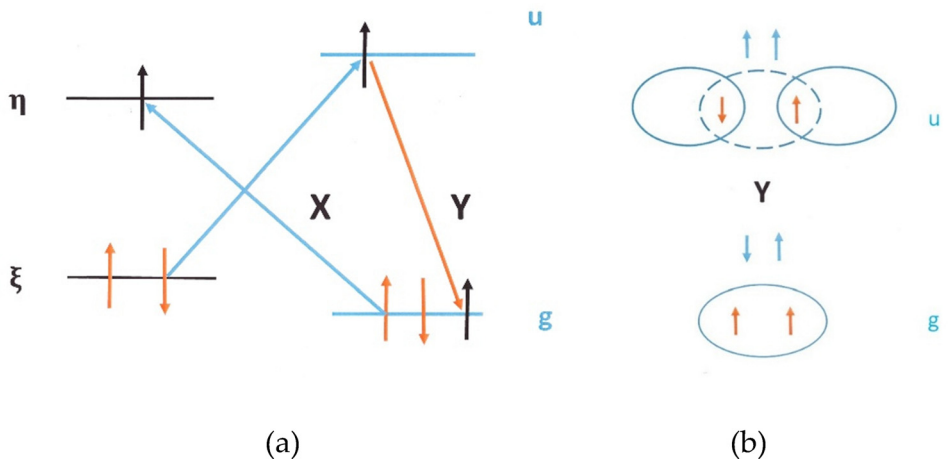

Fig. 3 Exchange–contact (XY) conversion process. The simultaneous electron exchange X and hyperfine contact Y of a hydrogen molecule interacting with a catalyst induces ortho–para conversion. (a) The molecule and the solid exchange an electron (X) and excite the molecule and the solid antibonding states. (b) In the next step the hyperfine contact (Y) induces a mutual electron and nuclear spin "flip-flop", inter-converting the molecule from a para state to an ortho one.

that the final reaction state was magnetic and that the previously accepted catalytic selection rule $\Delta S = 0$ should be extended to $\Delta S = 1$. Therefore, the metallic surface must have emitted magnetic quasi-particles during the conversion of the adsorbed molecules. The suggested mechanism was that at 10 K a conduction electron in the metal jumps from an occupied state to an empty one located above at 14.7 meV (the o–p transition energy). That new excited electron couples with the hole left behind and creates an electron–hole pair of "parallel spins", building a triplet pair of spin 1 that travels through the bulk. The H_2 conversion is conducted in two steps: one electric by excitation of the molecular antibonding 1 s state and the other magnetic conducted by the hyperfine contact that transfers the electron magnetic momentum to the molecular nuclear spins.

The Coulomb repulsion among surface complexes, either through electron exchange or charge transfers breaks the two molecular selection rules: the electron interaction transfers the orbital rotational momenta and the magnetic one the nuclear spin ones. The molecule–surface electron exchange was denoted as X, the charge transfer as U and the hyperfine contact as Y; the related conversion processes were correspondingly referred to as XY and UY.[46,47] The charge transfer process UY was found to be slightly faster than the electron exchange XY, estimated in between 1 and 10 min for (111) noble metal surfaces, and in between 20 min and 1 h for the bulk and (100) surface states. It was also predicted that a radiative excitation of the molecular surface layer would accelerate the conversion process. In 2003, 23 years later than the IBM observations (and 13 years after my interpretation) the Tokyo ISS team succeeded in measuring a conversion time of 13 min by REMPI on a polycrystalline silver sample at 15 K, and observed a slight acceleration by applying a laser beam.[48–50]

2.3.b Insulating dielectric catalysts. Since 2012, I have extended the XY and UY channels to insulating catalysts, first on metal organic frameworks, and then on amorphous solid water, silicon and porous polymers by considering a 3-stage process in which, in addition to dipolar or contact magnetic interactions and Coulomb electron repulsion, there is a third interaction between the catalyst's electron spins and their orbital motions.[51–55] The corresponding SCY conversion path for molecular hydrogen interacting with amorphous solid water is represented in Fig. 4 as an electron closed loop where only the nuclear o–p energy is transferred to the catalyst.

With the figures: $C \approx 1$ eV, $\Lambda \approx 3$ meV ($\approx$20 cm^{-1}), and $Y \approx 1.6 \times 10^{-6}$ eV, the conversion rate was estimated to be $\mathcal{P}_{o\to p} \approx 1.59 \times 10^{-3}$ s^{-1}, in remarkable agreement with the experimental value of 1.7×10^{-3} s^{-1}. The interpretation of the conversion patterns of molecular hydrogen adsorbed on amorphous solid water confirmed the electromagnetic nature of the process.[55]

For an assembly of hydrogen molecules diluted in a solid matrix such as silicon or inside porous catalysts such as "MOFs", I extended the electron basis to charge-transfer states inside a continuum of band states. The broadening of the antibonding molecular excited state by the solid conduction band provides efficient tunneling paths for hydrogen conversion. The conversion is induced by spin–orbital energetical fluctuations of the order of the eV, shared by the collection of the interacting sites. Triplet excitons are emitted and propagate until mutual annihilation.

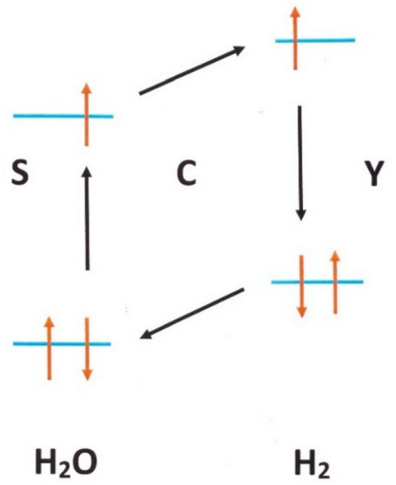

Fig. 4 SCY conversion channel for molecular hydrogen interacting with ASW. Spin–orbit S(Λ)—Coulomb repulsion C—and hyperfine contact Y: In this 3-step SCY channel, a first one-electron spin–orbit interaction S excites the surface water molecule into a 3s orbital perpendicular to the surface. The electron repulsion C with the hydrogen antibonding σ^*_u orbital induces then a simultaneous exchange of antibonding and bonding electrons. The last contact step Y relaxes the hydrogen molecule to its ground state, changing its initial ortho or para variety.

2.4 Energy and momenta exchange and transfers

This paragraph synthetizes the theoretical analyses of both static couplings and dynamic energy and momentum transfers between the interacting systems. Four quantum systems, the spin and orbital states of the molecule and catalyst electron and nuclei are admixed with the thermal variables. We have already discussed the impossibility to separate the molecular and surface electrons, but we must also underline the difficulty of separating the thermal variables and distinguishing between the catalyst considered as a thermostat and the hydrogen flow. In particular, it remains unclear whether the conversion energy is being transferred to the fluid or to the catalyst. Furthermore, this ambiguity persists even when the macroscopic isotherm or adiabatic experimental conditions are settled.

2.4.a Electron spin–orbit and nuclear spin–rotation couplings. The catalytic process that induces molecular conversion is characterized by a fundamental double o–p selection rule: $\Delta J = \Delta I = 1$. In the magnetic mechanism (M) both selection rules are satisfied simultaneously in a single step, whereas in electromagnetic channels (EM) they can occur in successive virtual steps. The (M) mechanism conserves the total electron spin $\Delta S = 0$, but (EM) channels transfer spin momenta $\Delta S = 1$ to the molecular rotation $\Delta J = 1$ and to the nuclear spins $\Delta I = 1$, in two steps.

The electron repulsion mixes bonding and antibonding electrons ("g–u"), transferring rotation momenta ($\Delta J = 1$)

towards orbital momenta, whereas the hyperfine contact introduces some electron spin excitation ($\Delta S = 1$), transferring spin momenta from the virtually excited electron to nuclear spin momenta ($\Delta I = 1$). This kind of exchange–contact channel can be observed in noble metal catalysis, where the nuclear conversion and the electron spin excitation are easily dissipated in the conduction band. For insulating or semiconductor catalysts, MOFs, ASW, Si, *etc.* the exchange–contact channel might be complemented either by the emission of triplet excitons or inter-band spin–orbit electron coupling. Spin–orbit splittings also influence the magnetic field effects observed in metallic oxide catalysis.

The electronic configuration of the surface structure plays an essential role in the conversion mechanism. 3d orbitals pointing perpendicularly to the surface certainly enhance the conversion rates and charge-transfer channels are certainly enhanced by very-high surface electrostatic fields with electrons getting closer and increasing repulsions. The induced dipole coupling to the electric field generated by all the oxide charges and interaction of the molecular quadrupole with electric field gradients split the rotational levels and the frustrated molecular rotation states at the surface become localized states in the angular degrees of freedom.

It is also important to emphasize the role of ionic species in the conversion channels: the oxygen ions for the MOF catalysis, and the OH ions for the transition metal hydroxides and the solid water (ASW) catalysts.

2.4.b Energy transfers. Hydrogen conversion might involve either electronic or nuclear transitions of various orders of magnitudes: nuclear rotational or vibrational energies <100 meV, or low electron excitation energies <500 meV. Higher electronic transitions of energies 1 eV induced by long range electron fluctuations can be shared by a number of adsorbed molecules, and such processes should be valuably examined with more details in the future. Various collective phenomena occur in the conversion mechanisms induced by solid catalysts.

2.4.b.1 Magnons. In 1970, I interpreted the efficiency of catalysts that exhibited some degree of ferromagnetism caused by emission of magnons that are able to accelerate the ortho–para transition of adsorbed molecules. As described in Section 2.2.3, when a magnon of frequency ω_q coincides with the ortho–para transition frequency, $\omega_q = \omega_{op}$, the molecule can relax to its para-state by emitting a spin-wave of that frequency. Oxides such as Fe_2O_3 or hydrous oxides $Fe(OH)_3$, $Mn(OH)_4$, $Cr(OH)_3$, $Ni(OH)_2$, and $Co(OH)_3$[41] which exhibit ferromagnetism were the very samples that exhibited the highest activity. In contrast, strong ferromagnetic materials such as Fe_3O_4, NiO, *etc*. are poor catalysts. On this basis I suggested a classification that favored ferrimagnetic catalysts that are more likely to satisfy the resonance condition. In a recent experiment, Fukutani *et al.* investigated the o–p conversion on a single-crystal film of Cr_2O_3 grown on Cr(110) with a laser technique of resonance-enhanced multiphoton ionization and observed a quite short conversion time estimated to be 210 s. The authors conclude that since the exchange interaction energy of the Cr ions is about 30 meV, the rotational energies of o-H_2 have possibly been dissipated into magnetic spin-wave energies (1–50 meV).[56]

Recently, synchrotron X-ray and neutron scattering data provided important information on the pair-distribution and pair–pair correlations of iron oxide and chromium oxide catalysts. The ferric oxide gel contains pair–pair correlations up to approximately 3 nm. The first three positive correlations can be ascribed to Fe–O, O–O, and Fe–Fe pairs. Such correlations can accommodate the spin fluctuations emitted by the hydrogen conversion. Without being ferromagnetic on a macroscopic scale, the ferric oxide gel has a large capacity to adsorb the o–p energy and distribute it among dozens of spin pairs for each adsorbed molecule.

2.4.b.2 Electron–hole pairs and excitons. For noble metal catalysis, after the observation at IBM labs that the ortho molecules deposited on a surface of silver (111) were converted into their para form in about 10 minutes, I demonstrated that the process emitted magnetic electron–hole pairs of triplet spin through the silver bulk.[46,47] My interpretation was confirmed by the Tokyo ISS team who measured a conversion time of 13 min by REMPI on a polycrystalline silver sample at 15 K. As also predicted, they observed an acceleration of the conversion rate by exciting the hydrogen antibonding state using a laser beam.[48–50]

For insulating catalysts the molecular conversion triggers the emission of magnetic exciton pairs that travel through the catalyst, before being disintegrated in a process similar to the ones observed in fluorescence.

2.4.b.3 Phonons. Quite generally, the thermal bath supplies (or absorbs) the o–p energy and maintains the thermodynamic equilibrium. The conversion energy is usually dissipated either through molecule vibration, kinetic desorption or interaction with solid-state phonons. Recently, Fukutani *et al*. investigated the surface temperature dependence of o–p conversions to study the rotational-energy transfer process. Such dissipation, discussed for physisorbed H_2 on amorphous solid water, silicate and carbon materials suggested that substrate phonons play an important role in the conversion. The two-phonon processes were shown to reproduce better the temperature dependence of the conversion rate than the one-phonon dissipation.[57–59]

3. Hydrogen catalysis: materials, phenomena and measures

Since the beginning of this century, novel structures have emerged that might build a new generation of ortho–para conversion catalysts. Their properties are being studied using novel radiative methods in research laboratories, Raman, Infra-Red, and Neutron vibrational spectroscopy or laser multiple photon ionizations.[16–20,48–50,60,61] The catalyst surfaces have been characterized by X-ray absorption fine structure (XAFS) and X-ray/neutron pair distribution function measurements.

3.1 Catalyst morphologies and structures

The Harshaw catalyst, chromia (20%) on alumina, has been used in cryogenic engineering laboratory liquefiers as a benchmark for the evaluation of the other catalysts. Among the efficient catalysts, ferric hydroxide gel and nickel silica gel are the most commonly used. Cr-doped silica (OXISORBs) contains 2–3% Cr(II) oxide on a silica gel carrier. Ferric oxide gel (IONEXs, Fe_2O_3) has a surface area of 200–300 $m^2\ g^{-1}$. Hydrous ferric and manganese oxide, unsupported, are obtained by gel precipitation, as Apachi-I, a highly porous nickel silica gel with a surface area of 500–600 $m^2\ g^{-1}$.[61] Other paramagnetic catalysts are obtained in the form of self-supported iron or chromium oxides[6,41,62–64] or multiple-decked sandwiches,[44] dispersed inside a porous zeolite[65] or attached to a MOF[66–68] or to a graphene oxide structure.[69] In particular, a series of various metal–organic framework M-MOF-74 catalysts (M = Mn, Co, Cu, Ni, Zn) studied first by FitzGerald in 2011 and recently by Polyukhov *et al.*[66–68] were found to be very efficient o–p catalysts with high porosities and accessible metal ion sites.

It is important to underline the fundamental role of catalyst pretreatments at high temperatures, but their various activation recipes remain empirical, as described in the excellent reviews.[70–73]

3.1.a Mesoporous materials. Since the sixties, Weitzel *et al.*[4] have conducted experiments on o–p conversion catalyzed by hydrous ferric oxide (30–50 mesh size) at a pressure of approximately 2.4 bar and temperatures ranging from 23.4 to 85.6 K. In their isothermal tests, hydrogen gas flowed through a small capsule containing hydrous ferric oxide and effluent o–p conversion was again measured using thermal conductivity. As detailed in Section 2.1.3 these thermal measurements at low temperature should be questioned. The original measurements were made with approximately 1/8-in. pellets. Later, powders with particle lengths of 2 mm and diameters of 5 nm, and even particles with sizes in between 300 and 600 μm were investigated, but fine powders present obvious disadvantages for use in liquefiers. Several powders, gels and catalytic beds have been tested. Currently, plate-fine or helical structural shapes are being explored.

Mesoporous materials have attracted substantial attention in the area of catalysis because they show unique magnetic, optical, electric, and sensitivity properties, quite different from the corresponding bulk materials. The conversion efficiency of amorphous and mesoporous Cr_2O_3 powders at a temperature of 77 K studied by J. H. Kim *et al.*[64] was attributed to their unique surface properties and high adsorption power. The external morphology of the catalyst post-treated at different temperatures and observed by X-ray diffraction patterns was found to be rod-shaped with a length of 2 μm and a diameter of 5 nm. Their macro pores of 7 nm in diameter, observed in the TEM image, were uniformly distributed inside the sample. X-ray diffraction patterns of Fe_2O_3 prepared by co-precipitation displayed the formation of highly dispersed a-Fe_2O_3 of increasing crystallinity with increasing calcination temperature. Particles of 16, 20 and 30 nm were observed at the calcined temperatures of 473 K, 573 K and 773 K respectively.[63,65,73]

More generally, porous MOF and amorphous structures possessing high surface area and intricate pore networks provide a new generation of catalysts.

3.1.b Surface structure of magnetic catalysts. The spin conversion process is dependent on various factors such as the BET surface area, calcination temperature and morphology of mesoporous catalysts. The surface area is the most important one since it conditions the number of molecules scattering the catalyst centers. All studies emphasize the crucial effects of high temperature pretreatment of their surfaces. Secondly the magnetic character of the paramagnetic catalysts is usually discussed in terms of the surface magnetic moments that characterize the interaction strength. The magnetic moments μ_{eff} of d^5 or d^4 configurations are about 5.92 or 4.90 Bohr magnetons, respectively.

The hydrous iron oxides which exhibited ferromagnetism were the very samples that showed the highest activity, about 5 times more effective than the chromium oxides. A similar pattern was also reported for Fe_2O_3 samples, although on a weight basis 0.5% Ni-alumina was even more active. On the Russian side, Buyanov in 1960 selected hydroxide gels with high surface areas of 100–300 $m^2\ g^{-1}$, with Cr^{3+}, Mn^{4+}, Fe^{3+}, Co^{3+}, and Ni^{2+} ions which have partly filled 3d shells. The best catalysts found in decreasing order of activity were Cr–Ni, $Fe(OH)_3$, $Mn(OH)_4$, $Cr(OH)_3$, $Ni(OH)_2$, and $Co(OH)_3$.[41] Weitzel *et al.*[62] confirmed hydrous ferric oxide ($Fe(OH)_3$), or ferric oxide gel, to be the most promising catalyst material.

3.1.b.1 Ferric oxide gel. Hydrous ferric and manganese oxides, when unsupported, are obtained by gel precipitation as Apachi-I, a highly porous nickel silica gel with a surface area of 500–600 $m^2\ g^{-1}$ whereas the ferric oxide gel exhibits a lower surface area of 200–300 $m^2\ g^{-1}$. (IONEXs, Fe_2O_3) was studied by Hartl *et al.*[61] The synchrotron X-ray total scattering data provided important information on the pair-distribution function (PDF) of the iron oxide and chromium oxide catalysts. Depending on the absolute Cr content on the silica surface and the surface properties of the silica support, different anchoring possibilities of Cr species were observed on a silica surface. Monochromatic species and dichromatic species can bind to the surface depending on the static charge of the surface during synthesis of the material. Dichromate species display closer range Cr–Cr interactions than the monochromate ones. The XAFS measurements on ferric oxide gel displayed a +3 oxidation state of iron in the material and a quasi-amorphous disordered structure. Neutron and X-ray scattering again provide complimentary weights to pair–pair correlations. X-ray scattering offers greater relative sensitivity to Fe bearing pair–pair correlations, while neutron scattering provides higher sensitivity to O-bearing correlations, and also sensitivity to the presence of H-bearing species. The ferric oxide gel contains pair–pair correlations up to approximately 3 nm. The first three positive correlations can be ascribed to Fe–O, O–O, and Fe–Fe pairs. The additional feature in the neutron data at approximately 1 Å can be ascribed to O–H pairs, indicating the presence of hydroxyl, H_2O or FeOOH species in the system. The real-space refinements attempted by Hartl *et al.* with

different phase structures of Fe_2O_3 and Fe_3O_4 models all fail to capture the features of the nanostructured gel. Significant residual intensity provides evidence for either an alternate structural identity or the presence of a secondary phase. A model combining γ-Fe_2O_3 and α-FeOOH provided a much closer match to the X-ray and neutron datasets. The authors conclude that models incorporating Fe–OH surface species on Fe_2O_3 nanoparticles might improve the fitting and provide further insight.

3.1.c Microporous powders and nano surgeries. Advances in molecular surgery have led to the development of novel techniques for open ligands in the MOF or carbon structures.[74–77] The pore size and hydrogen volumetric density optimization enable inserting another adsorbate surface within large-pore MOFs from the solution phase[75] (the large pores in MOF-177 have a diameter of 11.8 Å, which is sufficiently large). This was achieved through impregnation with a non-volatile guest or catenation with another similar framework. Besides reducing the free diameter of the pores, such guests provide additional adsorptive sites, thereby promoting the catalytic efficiency of the structure.

Rowsell and Yaghi were the first to describe these novel approaches for impregnation with reactive species through coordinative unsaturation.[76,77] This is possible with metal clusters that have additional terminal ligands with attractive secondary building units bound to them in certain MOFs. The solvent molecules coordinated to the metal may be liberated, and the terminal ligand may be removed without detriment to the framework, thereby exposing an open metal site to the void region. Another approach to construct MOFs with open metal sites is to embed these within a linker. Chemical modification with topology retention was reported for a series of Zn_4O-based MOFs;[77,78] it was noticed that the length and width of the linker appear to influence the hydrogen uptake at 77 K. A strong binding between H_2 and open Ni^{2+} has also been observed in open framework phosphate,[79] with these nickel-containing materials being particularly efficient in the ortho conversion of the hydrogen flow.

3.2 Hydrogen adsorption and diffusion

3.2.a Hydrogen rotation in adsorbed phases. The clear distinction between physical and chemical adsorption and catalysis, is fading since strong adsorbents and new precursor states (still in the physisorbed regime) have been observed for hydrogen molecules on a variety of MOF samples.[80,81] However in most cases when the molecular electronic bond is admixed with the catalyst electronic charge, its rotational momentum remains a good quantum number, although subject to some mixing with vibrational states. With rotation being hindered by the surface electric potential, the ortho and para energetical levels are split (see Fig. 1), and consequently the IR and Raman lines of adsorbed species present differences with the free molecular ones.

For the equilibrated spin isomers mixtures, it is common to define a separation coefficient $s(T)$ that measures the relative variation of equilibrium composition: $s(T) = \rho(T)/\rho_s(T)$, where $\rho_s(T)$ and $\rho(T)$ are the ortho–para equilibrium ratios, respectively in the modified phase and in the pure gas. Note that a factor $s = 16$ was measured on alumina in 1958[82] and the preferential adsorption of the ortho variety on a solid, compared to that of the para one, became a chromatographic method to separate the two varieties and a method to prepare enriched mixtures of the ortho variety.[83] Another important consequence, often underestimated, is that the equilibrium ratio of the two varieties is different on the surface of the catalyst from the gas one.

The most reliable methods to measure the relative content of the ortho and para varieties are now "*in situ*" spectroscopic experiments either by IR and Raman or by neutron vibrational spectroscopy (NVS). In a previous report by Hartl *et al.*,[61] "NVS" was used to characterize the hydrogen adsorption on the two most common ortho-to-para hydrogen converters: Cr-doped silica (OXISORBs) and ferric oxide gel (IONEXs). Comparing their patterns, the ferric oxide gel offers only one adsorption site for hydrogen. Hydrogen is bound strongly to the very polar ferric oxide surface (hindered rotation at around 60 cm^{-1}), as well as to the oxygen ions, and is not disturbed by the increasing amount of hydrogen present.

Distinctly, Cr-doped silica exhibits at least three adsorption sites for hydrogen. The hydrogen first adsorbs at the chromium sites showing a hindered rotation at 97 cm^{-1}. The band at the lower wavenumbers (70 cm^{-1}) indicates a strong interaction of hydrogen with the catalysts that can be caused either by 2–3 adsorbed hydrogen molecules aligned favorably at one chromium site or to the interaction of hydrogen with the silica surface while confined, *e.g.* in pores. Hydrogen on Cr-doped silica is less tightly bound than on ferric oxide gel. It is therefore easier to adsorb and desorb and the mobility on the surface is greater. The Cr-doped silica surface also adsorbs more hydrogen per surface area than the ferric oxide gel. The surface area of ferric oxide gel starts to saturate with hydrogen at loadings of approximately half a monolayer.

In experiments conducted by Hartl *et al.* various amounts of n-H_2 were loaded onto Cr-doped silica and ferric oxide gel catalyst to be measured by NVS, varying the amount of adsorbed n-H_2. Cr-doped silica and ferric oxide gel showed the same two peaks A and B for the hindered and free rotations. For chromia samples Peak A represents the hindered rotation of the hydrogen molecule on the surface of the catalyst due to a strong interaction. For higher loadings, peak A is split into two peaks: the first one (a_1) is observable around 70 cm^{-1} while the second peak (a_2) shifting from 80 cm^{-1} to 89 cm^{-1} is also present in hydrogen adsorbed on the surface of non-porous silica. The peak (a_1) is either connected to an interaction of more than one hydrogen molecule with the Cr-sites or connected to hydrogen adsorbing on inner-pore surfaces of Cr-doped silica while the peak at higher wavenumbers (a_2) exhibits less tightly bound hydrogen on a silica surface without geometric restrictions. The peak B of free rotational $J(0\text{-}1)$ transition in the spectra between 115 and 118 cm^{-1} increases in intensity with increased loading. Recall that the perfect rotor transition occurs at 118 cm^{-1}. The conversion was already complete in the time between loading of hydrogen on the sample and taking the first spectrum, which was at least 15 min.

For the ferric oxide gel the shift in the hindered rotation to lower wavenumbers is even greater than that for Cr-doped silica, showing a much stronger interaction between hydrogen and the electronegative surface. Peak A was found at energies as low as 56 cm^{-1} for the low loading and at 62 cm^{-1} for the higher loaded sample.

3.2.b Diffusion through the porous media microstructure. Numerous porous materials exhibit a variety of diffusive patterns through their labyrinthic frames. Efficient cryo-adsorption porous materials structured as activated carbon compounds,[84–87] or to be filled with powdered metal–organic frameworks,[76,77] are in use for the separation and purification of gases and even in fuel storage vessels for vehicles. Microporous adsorbents with desorption enthalpies in the range of $\sim$5–15 kJ mol^{-1} present a variety of pores, classified as micropores ($<$2 nm), mesopores ($\in$2–50 nm), and macropores ($\geq$50 nm). The pore size distribution of a cryo-adsorption material reflects the total density of the adsorbate molecules and not the total number of molecules within the plug.

3.2.b.1 Nano-porous activated carbon materials. Chahine and Benard initiated the adsorption studies of hydrogen on different nano-porous activated carbon materials and zeolites,[84–87] while metal–organic framework structures were further investigated and developed by Rowsell.[76,77] The activated carbon microporous materials AX-21, MOF-5, and MIL-101 have cage-like porous structures, rendering these efficient adsorbents for hydrogen applications, in particular for cryo-adsorbed vessels.[87] The adsorbent efficiency correlates with the specific surface area per unit volume of the adsorbent ($\in$0.2–1.5 $m^2\ L^{-1}$) defined by the product {specific surfaces ($\in$1.4–2.8 $m^2\ kg^{-1}$) $\times$ densities ($\in$0.15–0.51 kg L^{-1})}. The storage density value, comparable to the one documented for pressure vessels, could be reached at a pressure of just 60 bar if the container is filled with the pellets of super-activated carbon AX-21TM.

The surface areas of AX-21, MOF-5, and MIL-101 are on the order of 3000 $m^2\ g^{-1}$, while those of regular-grade microporous carbons are between 700 and 1800 $m^2\ g^{-1}$. High surface areas are an advantageous property for fast catalytic activity. The gravimetric density of hydrogen is approximately 100 g H_2 per kg of adsorbent, and its volumetric density is approximately 32 g H_2 per L in AX-21 carbons at 77 K and 50 atm. The preferred operating pressure for these sorbents (AX-21, MOF-5, and MIL-101) is less than 250 bar, a regime that utilizes the density benefit of the cryo-adsorbent prior to the exclusion density penalty becoming too large. In all sorbents, the stored hydrogen density is an increasing function of the storage pressure, with the effect increasing with decreasing temperature.

The simulation of hydrogen adsorption on single-walled carbon nanotubes and carbon slit pores with diameters ranging from $\sim$6 Å to 20 Å, performed by Wang and Johnson[88] at temperatures of 77 K and 298 K and in a pressure range of 1–100 atm, revealed that the materials were able to hold either one or up to five layers of adsorbed hydrogen. It was observed that the smallest pores held the most hydrogen on a per weight basis and per unit volume throughout the pressure range in which the simulation was performed. The smallest slit pore held a single layer of hydrogen, the highest uptake at the lowest pressures due to its strongest solid–fluid interaction potential. However, at higher pressures, the wider pores exhibited a higher storage capacity. At 77 K, the total amount of hydrogen adsorbed within the smallest pores remained constant throughout the pressure range and rapidly reached a value of 0.3 $cm^3\ m^{-2}$, which was close to the experimentally observed monolayer coverage of 0.32–0.35 $cm^3\ m^{-2}$. In contrast, the two largest pores were not filled completely even at a pressure of 100 atm. It was, therefore, clear that the optimum pore size for hydrogen storage depended on the storage pressure. At pressures greater than approximately 5 atm, the larger pores exhibited higher effectiveness because the weight fraction was dominated by the amount of available pore space at higher pressures. The storage capacity was much lower at 298 K compared to that at 77 K. At 298 K, the smallest pore was not filled completely even at a pressure of 100 atm, and the amount of adsorption was lowered by a factor of 6 (roughly) for the small pores.

3.3 Conversion measurements

A large variety of experimental setups are used to observe and measure the conversion processes and dynamics. Most of them are based on the nuclear properties of the hydrogen molecules, some are based on magnetic spectroscopy (neutron and NMR), while others are based on electric spectroscopies (IR and Raman). Differently, electronic properties have allowed laser spectroscopy (REMPI) to measure the nuclear conversion rates. All of them are more reliable than past thermal measurements which were restricted to static measurements of equilibrium samples. The present measures try mainly to select the best catalysts for effective liquefiers. Although the commercial Ionex catalyst is widely used and recognized as efficient, several research efforts focused on alternative catalysts. For example, Hutchinson[89] and Wilhelmsen *et al.*[90] found that a nickel oxide–silica catalyst doubled the catalytic activity of the iron(III) oxide.

3.3.a Nuclear spectroscopy

3.3.a.1 Neutron spectroscopy. Neutron vibrational spectroscopy (NVS) and neutron transmission (NT) are powerful techniques capable of probing a molecular layer interacting with a catalyst. It was shown in the previous Section (3.2.1) how neutron vibrational spectroscopy has been used to monitor the conversion rate of para to ortho hydrogen in the presence of catalysts. In particular, Hartl *et al.*[61] measured the vibrational density of states of parahydrogen and normal hydrogen in the solid state (10 K), the liquid state (18 K) and the gas state (25 K) at ambient pressure using neutron vibrational spectroscopy (NVS). The spectra showed that when neutrons interact with hydrogen molecules, a transition from p-H_2 to o-H_2 states J(0–1) can be induced even at low temperatures. In complement, neutron pair-distribution-function (PDF) analysis of Cr-doped silica and ferric oxide gels demonstrated that the structures are amorphous, with pair–pair correlations up to approximately 3 nm (30 Å) for ferric catalysts, whereas pair–pair correlations

almost completely disappeared below 15 Å for the chromia samples.

Energy-selective imaging using pulsed neutrons is used to provide molecular specificity beyond what is currently possible for *in situ* and kinetic studies, with direct industrial applications such as the well-known ''boil-off'' problem associated with the low-temperature storage of molecular hydrogen.

Neutron scattering is among the most-suitable techniques used to look at hydrogen in materials because neutrons can penetrate deep into bulk materials and allow *in situ* and nondestructive investigations. Moreover, the important difference in the scattering cross-sections of o-H_2 and p-H_2 for thermal neutrons makes energy-selective neutron transmission a unique technique to characterize the amount of hydrogen varieties in unknown mixtures.

Romanelli *et al.* used time-resolved neutron-imaging to characterize the ortho- to para-hydrogen conversion in condensed samples, in the presence of nanoparticles of γ-Fe_2O_3 acting as a catalyst. Experimental conditions were chosen so as to be representative of industrial applications, with the aim of providing additional insight into H_2 storage, and strategies to minimize the boil-off problem. They were able to characterize the conversion rate as a function of time and position of molecular hydrogen with respect to the catalyst. The results were reported for liquid and solid molecular hydrogen at 15 and 10 K, respectively.[60] They demonstrated how newly generated para-hydrogen poisons the catalyst, thus slowing the process and preventing the full conversion of large quantities of condensed molecular hydrogen, and underlined how the performance of the conversion critically depends upon the spatial distribution of the catalyst and on the loading procedure. Moreover, they suggested a honeycomb distribution of the catalyst in a vessel to boost the conversion rates, while minimizing the amount of material needed.

3.3.a.2 Nuclear magnetic resonance. Fig. 5 compares the ortho magnetic resonance lines to the much larger ortho–para conversion lines.

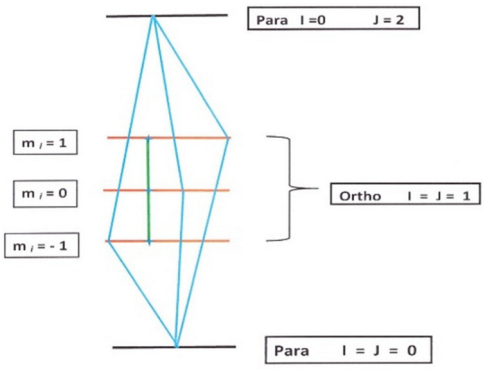

Fig. 5 Hydrogen conversion and nuclear magnetic resonance lines. The magnetic resonance lines in green are compared to the ortho–para lines in blue. The ortho manifold is amplified in comparison to the two neighboring para energies.

NMR measurements of ortho-to-para hydrogen spin conversion on solid catalysts are rare. Although NMR remains a powerful spectroscopy technique for gases or liquids, it remains rare for solid surfaces because of the limited number of molecules in adsorbed phases. An example of conversion measured by nuclear magnetic resonance spectroscopy (NMR) and free induction decay (FID) is given by the characteristics of amorphous and mesoporous Cr_2O_3 powders at a temperature of 77 K studied by J. H. Kim *et al.*[64] under a hydrogen flow. The mesoporous Cr_2O_3 catalysts prepared using mesoporous silica as a template and post-treated at 150C had the largest BET surface area of 230 m^2 g^{-1}. The external morphology of that catalyst post-treated at different temperatures and observed from X-ray diffraction patterns was found to be rod-shaped with a length of 2 μm and a diameter of 5 nm. They induced the highest o–p conversion, even superior to that of the commercial Fe_2O_3 catalyst. 13% of ortho hydrogen was converted into para hydrogen at 77 K in a continuous flow of normal hydrogen gas at a rate of 100 mL min^{-1}.[91] This highlights the superior efficiency of catalysts with low crystallinity. Another example was given by Polyukhov *et al.* (2022)[68] who studied various metal–organic frameworks (MOFs) as conversion catalysts by NMR to determine the rates at 77 K and 1 atm using a normal hydrogen feed at room temperature and ambient pressure. These frameworks have higher porosities and metal ion accessibilities compared to ferric catalysts. A series of M-MOF-74 catalysts (M = Mn, Co, Cu, Ni, Zn) were selected for kinetic studies and compared with the IONEX – type. It was concluded that, at 77 K, the Ni-MOF-74 was significantly more effective than other types of MOFs and Ionex catalysts. At lower temperatures with Ni-MOF-74 catalyst NMR could not register any remaining ortho-hydrogen in the reactor at 19 K. NMR spectroscopy was also used to observe the formation of molecular hydrogen diluted in silicon samples at various temperatures and the consequent o–p conversions.[17–19,92,93]

3.3.a.3 Infra-red and Raman spectroscopy techniques. Infrared (IR) spectroscopy is efficient for powders or porous oxides (such as MOFs), carbons and semiconductors. As a light molecule, the quantum characteristics of the nuclear rotation appear clearly in the resolved vibration–rotation lines, since the o–p splittings are different in the excited states. Raman or IR excitation bands contain a great deal of information because the coupling of nuclear-spin and angular momentum correlates with the arrangement of H_2 molecules in cage singularities, whether in the pores of polymers or adsorbed at metal, oxygen or organic sites of the metal–organic framework or diluted inside an interstitial site of a crystal.

The development of ''*in situ*'' and ''site-specific'' methods combined these new optical measures on a variety of diamagnetic insulators, with other surface spectroscopy techniques such as X-rays or neutron beams,[60,61] and thermal- or photo-induced desorption.[50] Metal–organic-frameworks and organic polymers became one of the best tools to observe the hydrogen conversion.[20] With hydrogen enriched in various ortho concentrations being introduced, o- and p-lines are clearly

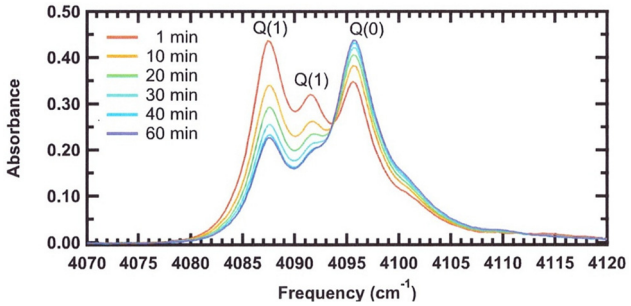

Fig. 6 Ortho and para hydrogen IR absorption lines in molecular organic frameworks. Ortho (red) and para (blue) lines of hydrogen adsorbed on MOF 74 sites. Ortho–para evolution in real time: the $Q(1)$ peaks decrease with time, while the $Q(0)$ peak increases (the legend gives time after loading H_2 into the sample chamber). Reproduced with permission from Burkholder, B., "Catalysis of Conversion Between the Spin Isomers of H_2 by MOF-74", Oberlin College, 2009 (also reproduced in ref. 20).

identified from their dynamical behavior. The simultaneous o-decrease and p-increase of these lines follow in real-time the isomers' relaxation towards thermal proportions as represented in Fig. 6.

"Site-specific" infra-red measures were achieved for hydrogen physisorbed in the pores of metal–organic frameworks (MOFs), by varying the amount of adsorbed hydrogen, and exploring and comparing the IR lines corresponding to molecules adsorbed on different metal, oxygen or organic sites.[20] The low-temperature diffuse reflectance infra-red spectroscopy technique conceived and realized by Stephen FitzGerald was used to measure the quantum dynamics of molecular hydrogen adsorbed in the micro-porous MOF samples. Measurements at low-temperature, with possible variable loading of hydrogen provide site-specific information. In particular, for MOF-74 samples IR measurements offered the additional possibility to correlate their conversion efficiency with their electronic distribution. It was a striking observation that the conversion rates over the metallic site and the oxygen one were of the same order of magnitude.[20]

The structure and morphology of synthesized catalysts are currently characterized by SEM, XRD, XPS, and Raman spectroscopy analysis. The methods used by T. Das *et al.* to synthesize nano-sized ferric oxide particles were microemulsion, precipitation/co-precipitation, sol–gel, electrodeposition, and the surfactant-mediated method.[63] The catalytic properties of iron oxide nano materials were improved by controlling the method of synthesis, the solvent nature and pH, supports, polymers, type of surfactants, added electrolyte, reagent concentration, nature of the precursors used, and heat treatment during synthesis. In particular, the solvent has a significant role in controlling the sizes of nano materials. A series of α-Fe_2O_3 catalysts were prepared by precipitation, and by varying calcination temperatures, solvents, and precursor concentrations. The liquid-phase spin conversion performed by *in situ* FTIR spectroscopy at a cryogenic temperature of 17 K was shown to be affected by the catalyst′s calcination temperature, initial precursor concentration, solvents used and the precipitating agent, but the highest catalytic activity was found for samples containing hydrated $Fe(OH)_3$ or FeOOH during the synthesis of α-Fe_2O_3 at 393 K. Comparatively, alumina-supported iron oxides exhibited a much slower spin conversion.

An illustration of the use of Raman spectroscopy to analyze the conversion process is provided by the behavior of the hydrogen molecules in nanocages as observed in nanosized porous coordination polymers (PCPs). The conversion of ortho (o)–para (p) nuclear-spin isomers was measured through the temperature dependence of the Raman spectra.[94] A correlation between the nuclear-spin populations and the structural change in the H_2 arrangement observed by X-ray diffraction was established. Raman spectra allow us to monitor the progressive loading of the molecules on various sites, while the ortho–para patterns could be correlated to the charge density measurements in the pores considered as electric nanocages in which the H_2 molecules are physically trapped. Three H_2 sites were found but the molecules cannot coexist in all sites in one pore, since the inter-site distances are too short. The shortest distance between two H_2 molecules in the pore was estimated to be 3.0 Å and the molecules cannot be accommodated necessarily at equilibrium positions. The different arrangements of the molecules in a pore were followed by the Raman bands as the temperature was decreased by cooling from 77 to 20 K. Changes were found in the intensity and peak positions and the authors underlined such correlation between the electric distribution and preferential sites. The catalytic hydrogen o–p conversion was found to occur preferentially at the sites characterized by intensive electron charges densities.

3.3.b Electron spectroscopy. The first electronic method to observe the rotational states of hydrogen molecules adsorbed on surfaces was realized by EELS (electron energy loss spectroscopy) measurements in 1982.[32,33] First, P. Avouris at IBM labs reported that the ortho molecules deposited on a surface of silver(111) were converted into their para form, in the time of about 10 min necessary to run the apparatus.[14] Shortly after, S. Anderson in Chalmers observed a slower effect on Cu(100).[15] A similar effect was reported later on graphite.[16] In all cases, the rates were too fast to be recorded and had to await the Photo-Ionization method, called "Resonance-Enhanced-Multi-Photon-Ionization" (REMPI). This method developed at the beginning of the new century is different in nature from the IR "*in situ*" ones, as it involves a first step of desorbing the molecules before their analysis. Moreover, the laser measurement explores the rotational energies from the top, from the vacuum energy threshold.[48–50] In the REMPI method, the hydrogen molecule is first excited through the transition $X \rightarrow (E, F)^1\Sigma_g^+$ by two-photon absorption and then ionized by another photon. The electronic excitations are able to characterize the ortho and para hydrogen states because of their different excitation energies.

The concentration of hydrogen spin isomers adsorbed on solids measured by REMPI must be combined with desorption techniques. Photo-Stimulated Desorption (PSD), or Thermal Desorption (TDS), ejects the molecules from their adsorption sites before being probed by the laser beams. The preparation

of non-equilibrium ortho-hydrogen is realized by chromatography. In 2003, the first precise experiments of hydrogen physisorbed on Ag(111) at low temperature, based on photodesorption and molecular ionization, were realized by REMPI using a laser beam of 2.3–6.4 eV. A conversion time of a few minutes was recorded (as predicted by my theory[46,47,95]) and the rate was accelerated by increasing the laser power (as also predicted). Shortly later, o–p conversion of hydrogen adsorbed on amorphous ice (ASW) by the same REMPI method was also observed to be quite fast and on the similar order of a few minutes. As described in the previous theoretical Section (2.3), I was led to introduce a third virtual interaction, a non-diagonal spin–orbit coupling, to the XY exchange contact process in order to explain the fast conversion rate. With regard to the dynamical aspect, Ueta and Fukutani introduced a two-phonon process for the energy transfer towards the catalyst to explain the temperature dependence of the conversion rate.[57–59]

To conclude on the main characteristics of catalysts that must be taken into account in industrial applications and, in particular, in controlling the hydrogen space velocity through liquefiers catalysts, I shall stress the importance of highly polar oxide surfaces as efficient conversion catalysts, and their disordered or amorphous structures.

4. Catalytic functions in liquefaction and storage

Catalysts have become essential parts of hydrogen liquefiers.[71,72,89] The slow transformation of ortho-to para hydrogen is one of the barriers to long-term liquid hydrogen storage given that the heat of conversion can evaporate more than 70% of the stored liquid hydrogen. Since the conversion from normal to para-hydrogen is exothermic, it releases more heat (525 kJ kg^{-1}) than the enthalpy of vaporization (448 kJ kg^{-1}), at liquid hydrogen's normal boiling point. Consequently, the ortho–para conversion of hydrogen is extremely important for industrial-scale applications of hydrogen liquefaction and storage. Normal hydrogen that is liquefied too rapidly will generate excessive amounts of boil-off gas. Excessive amounts of boil-off gas may cause over-pressurization of the cryogenic storage tank, leading to serious safety issues.

The rational way to promote the use of hydrogen energy would be to integrate the production, storage, distribution, dispensing and consumption processes. The efficiency of liquefiers is mainly estimated according to the production of liquid hydrogen, but the process is energy-intensive and excessive costs hinder its uptake in industry. An important part of the production only needs short term storage which must be considered when profiling the catalytic requirements.

Hydrogen liquefaction and liquid hydrogen storage are inverse processes, although complementary. The insertion of elaborated microporous catalysts might also play a key role inside future storage tanks. Three characteristic material parameters are decisive in ensuring three necessary catalytic functions: the porosity regulates the capillary flow of hydrogen, the electromagnetic surface governs the electronuclear reaction, and the conductivity determines the thermal exchanges. However, they respond in opposite ways in the two inverse devices. The flow must not be obstructed inside liquefiers, whereas it must be slowed down in storage vessels; the catalytic conversion emits energy during the cooling process while it absorbs environmental heat during storage, and the pressure drops are a harmful inconvenience in liquefiers, while advantageous for producing necessary expansions in the delivery process of hydrogen vessels. The porous content, electromagnetic strength and thermal conductivity of the nanomaterials should advantageously be adapted to the particular catalytic, heat exchange and pressure expansion functions required at each step.

There are numerous excellent reviews about the liquefaction processes.[71,72,95–98] Herein, I concentrate on a few catalytic effects and challenges related to the production of liquid hydrogen and in relation to short storage periods (one or a few days). Long term storage and intermediate storage (a week or so) are beyond the scope of this paper.

4.1 Catalysis and space velocity in liquefiers

It is important to recall a few orders of magnitude of the volume rate constants (in min^{-1}, normalized by the H_2/catalyst weights ratio) are required to convert a given amount of hydrogen. Karlsson[99] used IONEX catalysts to convert normal hydrogen in a flow loop at 20 K to 99.8% para-hydrogen in 0.128 min^{-1}. Zhuzhgov *et al.*[97] also estimated that converting normal hydrogen to 99% para-hydrogen at 21 K in a continuous flow reactor filled with Fe_2O_3 catalyst (like IONEXs with a void fraction of 0.38) was completed at a rate of 0.02 min^{-1}.

It is important to note that nickel oxide catalysts when dispersed on a diamagnetic catalyst might even achieve faster rates. For instance, NiO on Al_2O_3 as a catalyst at 22 K is about 10 times more efficient than $Co(OH)_3$ at 78 K.

But why is it important to reach faster rates?

4.1.a Objectives. One of the key challenges of the hydrogen liquefaction plants is to combine the heat exchange and converter units. The present tendency is to insert the catalyst into plate fin thermal exchangers that accommodate both direct and recycling counter-currents. Continuous ortho-to-para conversion in commercial hydrogen plants, was promoted in an early evaluation by Lipman *et al.*, on a theoretical basis.[29] The reversible process requires less additional work and this kind of continuous conversion is approached in catalyst-filled PFHXs.

Specific energy consumption for continuous-conversion is 21.8% and 28.7% lower than for adiabatic and isothermal based processes.[98] Continuous conversion heat exchangers require converting the parahydrogen content to over 95% within a limited temperature range, typically 80–20 K. This requirement presents a great challenge to large-scale liquefiers that need to handle the large-flow rate hydrogen with an acceptable pressure drop.[100] The design of a plate fin heat exchanger filled with a conversion catalyst presents significant challenges including turbulent flow in the cold flow channel, while catalyzed conversion is performed in the catalyst-filled

hot and porous channel, together with simultaneous heat transfer between the cold and hot channels. How these mechanisms interact with each other is not fully understood.[101]

In terms of heat transfer, cold media are used to remove both heat generated from the conversion and the latent heat of the hot media. For sure, more heat is used to remove the latent heat of hydrogen than the conversion heat, but the catalytic process introduces additional work and constraints. Reports[71,72,96] have stated that ''It is in fact likely that the ortho–para conversion kinetics in many practical scenarios are limited by heat transfer in terms of the removal of the heat of conversion''. However, O'Neill *et al.*[102] found that the outlet parahydrogen fraction is ~10 times more sensitive to reaction rate kinetics relative to heat transfer, and suggested the reactor geometry should be primarily determined by conversion kinetics. The choice and control of the space velocities present conflicting outcomes where an improvement in heat transfer coincides with a decrease in the catalytic efficiency with an increase in hot flow velocity.[101] Increasing the flow rate of the cold channel enhances the heat transfer but does not have any positive effects on catalytic efficiency. The heat release elevates the local temperature within the catalyst channel, creating a stronger driving force for heat transfer between the hot and cold channels. At lower cold flow rates, increased kinetic parameters may make heat transfer the limiting factor. In such cases, enhancing the heat transfer by increasing the cold flow can improve the catalytic efficiency.[98,100–103]

Mendoza *et al*. found that that if conversion is carried out simultaneously with the cooling of hydrogen it can yield up to 22% and 29% energy savings compared with adiabatic and isothermal conversion, respectively.[30] They compare catalytic conversion conducted either with a perfect catalyst or an imperfect catalyst occurring simultaneously with the cooling process. The conversion with a perfect catalyst represents the conventional idealization, assuming that hydrogen reaches the o/p content dictated by thermodynamic equilibrium instantaneously with temperature changes.

The conversion with an imperfect catalyst represents the use of a common catalyst with suboptimal activity, resulting in a slower and delayed conversion. To produce LH_2 with the same o/p content as in the thermodynamically controlled process, the conversion with an imperfect catalyst requires cooling of the H_2 feed to a lower temperature than the one needed with a perfect catalyst. Producing 99.6% LpH_2 costs between 25% and up to 57% more energy compared with LnH_2 (without conversion) respectively, depending on where the conversion is performed in the process and how effective is the catalyst. Consequently they concluded that full (99.6% para-hydrogen) ortho–para conversion is impractical, leading them to suggest that partial conversion might be enough for practical use of hydrogen energy, as was already demonstrated by Baker and Shaner of the Linde corporation in 1978.[31] From a theoretical point of view, one ortho molecule left in the liquid would convert many neighboring para molecules into ortho ones! Thermodynamical equilibrium requires long range interactions whereas o–p conversion is of very short range. Increasing para content above 99% para-hydrogen is extremely difficult, costly and of limited interest in avoiding evaporation losses, particularly if the liquid is rapidly transformed into chemical or electrical energies.

Another important complexity presenting conflicting outcomes concerns the pressure drop associated with the barrier introduced by the insertion of catalysts within the liquefaction process. Park *et al.*[104] studied the pressure drop in a catalyst-packed heat exchanger using a cylinder filled with commercial IONEX catalysts. It was found that the pressure drop is almost linearly dependent on space velocity. Reducing such catalyst-induced pressure drops may prove to be a crucial feature of increased liquefaction efficiency. Moreover, several important questions remain unanswered; these include the optimal operating conditions, the best catalyst activation procedure, the catalyst deactivation mechanisms and the rate.

4.1.b Reaction kinetics. The macro-kinetic principles of the catalytic hydrogen conversion on a solid catalyst follow a few consecutive steps of heterogeneous catalysis: diffusion between the fluid, the catalyst pores and surface, adsorption and conversion at active surface sites.

Weitzel and co-workers found that film and pore diffusion effects are negligible for hydrous ferric oxide under common cryogenic operating conditions. Furthermore, the authors suggested first-order kinetics, assuming that adsorption and desorption processes are also insignificant. This simplification was supported by several other authors,[72] but deviations from simple first-order kinetics were observed for hydrous ferric oxide as well as for the highly active NiO catalyst. Hutchinson *et al*. applied Langmuir–Hinshelwood kinetics and found satisfying correlations derived from theory, which included adsorption and desorption effects for conversion over hydrous ferric oxide,[89] revealing deviations from first-order behavior.

Donaubauer *et al.* compared the first-order and the Langmuir–Hinshelwood kinetic approaches for the reaction rate.[105] Hydrous ferric oxide was chosen as the catalyst. For this, experimental datasets published by Weitzel *et al.*[4,25,62] and Hutchinson[27,89] were used. When neither adsorption nor desorption processes are considered and only the surface reaction is accounted for, the first-order rate constant does not depend on the molar concentration, in contrast to the Langmuir–Hinshelwood model that implies uniform surface coverage. Equilibrium composition was estimated using hypotheses that might be questioned (a rigid rotor model and only initial slopes were considered). Both deviations in catalyst activity and different operating ranges in the two studies became apparent. Due to the inherent deviations of the datasets, kinetic data fitting could not be achieved by simultaneous fitting of all data points.

A recent, updated and complete review of experimental datasets, for the catalyzed ortho–para hydrogen conversion reaction, discusses the catalytic activity and cost-effectiveness as a function of the space velocity of the feed stream across a catalyst located in a reactor cell.[72] Their objective is to provide validation for the use of conversion kinetic models, derived from the experimental datasets, to support a hydrogen liquefaction

design and to quantify the sensitivity of this design to current reaction kinetic parameter uncertainties. It highlights the sparsity of experimental conversion data under relevant cryogenic conditions and the need for a more comprehensive and fundamental understanding of the origins of the spin conversion catalyst effect and how it is impacted by various deactivation mechanisms.

It starts with the experimental data obtained from Hutchinson's reaction kinetic apparatus and reports the para fraction of a hydrogen mixture passing through a ferric oxide gel catalyst as a function of space velocity defined as the volumetric hydrogen flow rate per unit bulk volume of catalyst. It is complemented by various datasets extracted from earlier studies on different catalysts by Weitzel *et al.*,[4] Falcão *et al.*,[96] Wakao *et al.*,[6] and Buyanov *et al.*[41] and by their own measurements obtained using a more refined apparatus. The setup enabled measurement of the converted hydrogen exiting a mini-reactor cell at a controlled temperature of 77 K *via* the use of *in situ* Raman spectroscopy.

Conversion kinetic data acquired for a hydrous ferric oxide catalyst were found in reasonable agreement with the limited existing literature, and these authors concluded that (i) the most common commercial catalyst, the ferric oxide gel, satisfies *quasi* optimal performance requirements and (ii) the conversion reaction remains first order in the isomer products while diffusing through the porous solid structure. However, their conclusions are tempered by observing that available conversion kinetic data are sparse under liquefaction conditions of temperature and pressure for both ferric and non-ferric catalysts, and that a much more comprehensive array of reaction kinetic data is required.

The model proposed by Wilhelmsen *et al.* was found to be more accurate than the Langmuir model at higher ortho-content and low conversion levels.[90] Given that the thermal conductivities of para- and ortho-hydrogen differ by only 4% at 300 K, the reliability of these measurements is significantly impacted, particularly at low temperatures. While investigating a catalyst-filled PFHX design in the temperature range from 47.8 K to 29.3 K, they reported that thermal gradients and the ortho–para-hydrogen conversion are the two major contributors to exergy losses in the system.[90]

The question remains open as to the relative importance of hydrogen diffusion and adsorption through the porous catalysts and to conclude what is the rate controlling process.

4.1.c Irreversibility. Differences in thermal conductivity have been used as a basis for measuring the ortho–para ratio in a sample of hydrogen, particularly in the temperature range of 50 to 250 K. However, such reference calculations and thermodynamic property measurements cannot be simply extended to non-equilibrium ortho and para mixtures even when the ortho–para ratio is known as a function of time (*e.g.* using Raman spectroscopy), as demonstrated in the theoretical section (2.1.c). This is also true for the transport properties of arbitrary hydrogen mixtures. Models for the viscosity and thermal conductivity of hydrogen are needed to estimate, respectively, pressure drops and heat transfer coefficients in various unit operations within the liquefaction process (*e.g.*, cryogenic heat exchangers) when the hydrogen flow is not completely equilibrated.

Let me first discuss a few measurements and related conversion concepts. Fig. 7 qualitatively represents the experimental para content at the outlet of the catalyst as a function of residence time t of hydrogen in the reactive conversion cell. In particular it might correspond to two different series of measurements obtained by Hutchinson with two initial hydrogen compositions: (i) a normal mixture, n-H_2, prepared at room temperature and (ii) almost pure parahydrogen gas prepared at 20 K, both flowing across a ferric catalyst maintained at a temperature of 77 K. Jiao *et al.* represented such para contents at the outlet of the catalyst as a function of the hydrogen volumetric flow rate in Fig. 4 of ref. 72. That space velocity depends on the feed stream, and is thus inversely proportional to the time spent by hydrogen in the conversion cell.

Since there is a deficiency of conversion data below 77 K and above 0.24 MPa, it is often assumed that o → p and p → o reaction data might be compared. The para content is described in the normal mixture as increasing from o → p conversion. In a para stream, it is described as decreasing from a back p → o conversion. This kind of qualification and comparison between direct and back conversion might be confusing since the initial content, being prepared at different temperatures, 300 K or 20 K, has different compositions.

At any temperature, both o → p and p → o reactions coexist; however, the reactions differ when the initial compositions of isomer mixtures vary (for instance, the levels J = 2, 3,... contribute at 300 K but not at 20 K) and this distinction is particularly relevant when the hydrogen flow does not reach an equilibrium with the catalyst temperature.

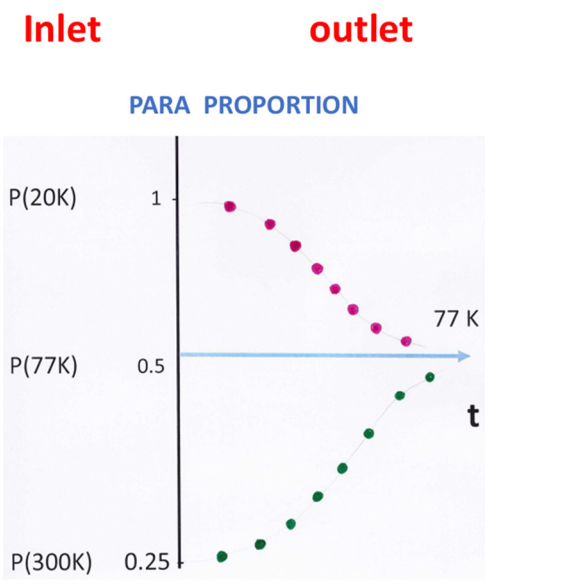

Fig. 7 Para proportion in a hydrogen flow. The para proportion of a hydrogen flow is represented as a function of the residence time t the hydrogen spends in the reactive conversion cell (arbitrary units are a function of pressure). Inlet proportions correspond to the experimental conditions (catalyst at 77 K).

Representation of the conversion as a function of space velocity is also confusing since with increasing space velocity an increasing number of molecules avoid contact with the catalyst, reducing the extent of the conversion process. The described experiments are more representative of a lack of reaction rather than of a conversion as a function of time. A lack of conversion in a flow differs from the partial conversion of an adsorbed hydrogen layer on a catalyst surface acting as a thermostat.

At the start of the experiment, the hydrogen behaves as an equilibrated gas prepared either at 20 K or 300 K, but as soon as it passes through the catalyst it becomes a mixture of 2 different gases, where each component tries to accommodate separately to the catalyst temperature (here 77 K). However, the molecular ensemble does not reach a state of equilibrium with the catalyst, unless the space velocity is very slow. In contrast, it undergoes an irreversible transformation after the hydrogen mixture has been prepared at an initial temperature T_0 = 300 K or 20 K (initial state only imperfectly defined) and crosses a catalyst at T = 77 K during a time t without reaching equilibrium in most cases. The o–p ratio, being a function of the 3 variables (t, T_0, and T) is insufficient to define a state! It lacks knowledge of at least the first 4 levels of populations or other thermodynamical potentials, such as entropy.

Consequently, the upward and downward curves cannot represent the o → p and p → o reaction rates in a phase space and cannot model conversion kinetics. Each successive point is a representative but not a line. In particular, the para content reached at time t_1 is a function of time t_2 ($>t_1$) necessary to reach equilibrium. If assumed that the para content is a continuous function of the 3 variables p (t, T_0, T), 2 regions of opposite concavities in Fig. 7 should be distinguished. For the pure para initial stream, the first region $p \leq 0$ corresponds to a separate equilibrium where each variety, its ortho and para components, equilibrates at the catalyst temperature but not with each other, whereas in the second longer period, characterized by $p > 0$, the flow tends towards a global equilibrium (and inversely for the normal initial mixture). However, such a simplified picture should not be taken too strictly since these kinetics are intricately mixed.

4.1.d Discussion. Many processes are at work, some compensating others, for example energy exchanges and preferential adsorption. It is well known that the ortho molecules adsorb more easily on surfaces which enrich the stream in para molecules arising either from the escaping molecules or from the converted ones. The conversion process itself varies with the temperature and pressure of the flow. With decreasing space velocity, more molecules adsorb on the catalyst surface and within the micropores, resting also longer in contact with the catalytic centers, their conversion increases.

The investigation of the heat exchanger model showed characteristic features of the ortho–para hydrogen conversion in counterflow PFHXs.[90,105] The catalytic conversion is mainly driven by the equilibrium ortho-content which is a function of the reacting side temperature. Therefore, the ability to cool directly determines the conversion and while the residence time of the reacting stream in the respective catalyst volume is an essential parameter, it is not sufficient to define the conversion process.

The illustrated operating range for supercritical hydrogen liquefaction highlights the difficulty of kinetic evaluation. While high-pressure configurations allow better thermal heat transfer they do not necessarily enhance the conversion rate. This depends on the temperature range and on the conversion process. For instance, evacuation of the reaction energy by the phonons is enhanced by increased residence on the catalyst surface. There is almost no overlap between experimentally approved catalyst activity and the operating range.

Raman spectroscopy is a crucial tool used to study and disentangle the various catalytic processes, by measuring the different populations of the rotational levels of the ortho and para varieties, *in situ*, at different stages of the liquefiers.

4.2 Catalysts for intermediate and short-term storage

A thermally isolated tank of liquid normal hydrogen will lose, from internal conversion, about 18% of its volume during the first day of storage, 40% after 100 hours and 60% after 300 hours. For storage of a higher para proportion of liquid, the storage duration is increased proportionally. It is therefore necessary to store liquid hydrogen containing a large proportion of para variety.

In open systems for hydrogen liquefaction and storage, a new generation of catalysts is also needed to adapt heat exchange, expansion and magnetic conversion functions to fast flow and temperature conditions. An open system (in the thermodynamical sense) is a system which exchanges heat, matter and radiation with the environment. Storage of LH_2 in a vessel is a non-equilibrium and unstable system which receives heat and radiation from the environment and delivers matter to the fuel cell.

The greatest engineering challenge associated with hydrogen mobility is storing enough hydrogen onboard the vehicle for a reasonable range (500–1000 km). Today's hydrogen-powered ground vehicles mainly use compressed gas storage, at pressures typically of 350 or 700 bar with fully wrapped high strength carbon fiber (Type III or IV) vessels.[106–108]

4.2.a. Cryo-compressed and cryo-adsorbed storage vessels. The best cryo-compression and cryo-adsorption storage vessels reached the 2017 weight and volume targets promoted by the US Department of Energy: a volumetric capacity of 45 gH_2 per liter of vessel and a gravimetric capacity of 7.5%.[109–113] Nearly all LH_2 storage vessels use metallic double-walled containers that are evacuated and contain multiple layers of alternating metallic and thermally insulated polymeric or glass films to reduce heat leaks to the cryogenic fluid *via* convection, conduction and radiation. The vacuum space contains numerous sheets of highly reflective metalized plastic. These storage vessels are heavy, bulky and expensive. They imply excessive mechanical containment and intensive thermal insulation[112] and consequently important investments in their manufacture, production and maintenance costs. But is it necessary? Or more precisely to what extent? The following model presents an alternative ''short term'' hydrogen storage vessel.

4.2.b Double open hydrogen vessels: principles and structure. The concepts of open systems and of vessels embedded within one another, in which a multiple barrage system is inserted, are based on the cryogenic, cybernetic, hydrodynamic, and catalytic properties, currently adopted to liquefy hydrogen in the industry. While combining the same thermal functions they operate in opposite directions. A schematic three-walled structure with a counter-current and multiple catalytic plugs as an example of Double Open Hydrogen vessels, DOV, is represented in Fig. 8.

Their main patterns are: open, presenting adjacent countercurrents and including a barrage system[32] as summarized in Fig. 9 and 10:

– Open, in the sense of immediate and continuous flow. The unique valve located at the vessel exit regulates the hydrogen current towards the fuel cell. Toyota's recent hydrogen cars use initial boil-off gas to load the battery.

– The DOV vessels use embedded and connected containers between which the hydrogen gas flows, as currents and countercurrents. In such a device, the incoming thermal heat, which initiates liquid evaporation, is transformed into a directional flow of hydrogen. The last countercurrent, being the most heated, is the first evacuated.

– These storage vessels include a barrage system of successive microporous plugs cumulating in multiple functions: (i) mechanical support, (ii) gas expansion and flow control, (iii) adsorbing and (iv) catalytic activities.

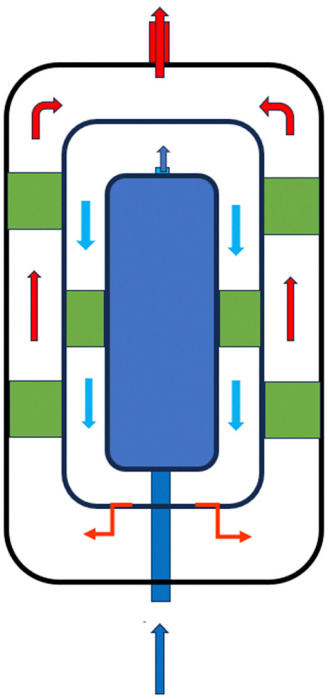

Fig. 8 DOV compartments and the hydrogen flow path. Hydrogen schematical flow path of a typical DOV reservoir with a three-walled structure. Hydrogen load, reservoir and currents (in blue), counter-currents and outflow (in red) and multiple microporous catalytic plugs (in green).

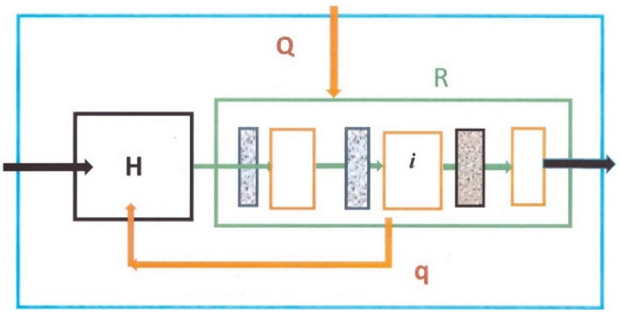

Fig. 9 Retroaction scheme in DOV storage vessels. LH_2 is loaded in *H*. Part *q* (in brown) of the entering heat flux (*Q* in brown) reaches the reservoir *H* inducing a directional hydrogen current (in black) that crosses the microporous catalysts (in grey) and is directed towards the fuel cell. By reversing the arrows, the flows in the liquefiers can be schematically represented.

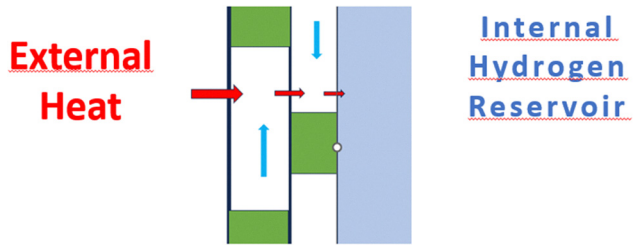

Fig. 10 Matter and heat fluxes in DOV storage vessels. Hydrogen currents and countercurrents are represented by blue arrows, and heat flux by red ones (catalysts in green also adsorb part of it). In DOV devices, part of the incoming thermal heat, being at the origin of the liquid evaporation, is transformed into a directional hydrogen current, while another part is evacuated by the countercurrent.

The hydrogen flow regulation is achieved through a barrage-system of successive porous plugs with decreasing porosities. These inserted materials combine four functions: (i) mechanical support rigidifies the double structure, (ii) successive JT expansions stabilize the flow and delay the pressure and temperature increases, (iii) a variable adsorption–desorption cycle, and (iv) hydrogen catalyzed conversion transforms part of the translational motion into spin–rotational internal energy.

The inner reservoir initially filled with liquid hydrogen, subjected to the highest pressure must be the most rigid, but successive separation walls might be thinner since they are exposed to hydrogen pressurization forces of lower intensities and opposite direction. Along the hydrogen current, each microporous plug retains some molecules and initiates a cascade, producing a JT expansion that reduces the pressure in the following compartment. Thus, at any instant, the pressure drops in both the longitudinal and transverse in → out directions. The time evolution of the hydrogen current can be divided into the 4 following periods: (I) loading and boil-off, (II) pressure build-up, (III) steady flow and (IV) back-off, of successive physical phases (liquid, fluid mixture, and gaseous).[32]

The first phase lasting a few minutes corresponds to the loading (20.4 K) at high density ($\sim$80 g L^{-1}) into an inner

H-container. Insertion of that H-container inside a larger one decreases the hydrogen density to $\sim$60 g L^{-1}. In the second phase of pressure build-up, hydrogen undergoes a sharp increase in its pressure and temperature; however these increases become progressively limited by the resulting JT expansions, the ortho spinning of the converted molecules, the feed dilution due to continuous gas ejection and the micropore fillings in the nano materials. The system reaches a quasi-steady flow in a third phase when the decrease in hydrogen density due to gas ejection compensates for the increase in temperature. The pressure of the internal container reaches a plateau in between 120 and 140 isobars. In the last back-off phase, from 130–150 K, the flow is sustained by desorption from the plugs.

4.2.c Break-even times for storage processes. It appears of particular interest to enlarge the concept of break-even times, introduced by the Linde Corporation in 1978.[31] In hydrogen liquefiers, for each initial composition a break-even time exists at which the energy cost of conversion equals the energy cost of the vaporized hydrogen. If the hydrogen is used within the breakeven time, partial conversion is advantageous with respect to energy consumption. For example, a breakeven time of 19 hours was observed for normal hydrogen and 36 hours for 48.5% para hydrogen.

Mendoza *et al.*[30] considered storage time in two ways: (1) the time before 1 wt% of the initially stored LH_2 vaporizes due to conversion heat and (2) the time for which the energy cost associated with conversion heat removal is matched by the cost of LH_2 replenishment to cover for the boil-off losses. The storage time with minimum losses is thus investigated in terms of energy cost for liquefaction. They termed ''conversion energy-recovery time'' the range of time for LH_2 usage when partial conversion (for p-H_2 $<$ 99.6%) is advantageous. Considering that the energy requirements and exergy losses associated with greater conversion in the higher para range are more significant than foreseen with idealized conversion studies, they evaluated levels of conversion that are appropriate for specific LH_2 applications. They found that at low para concentration a 12% increase from 25% to 37% results in 2–8% higher specific energy consumption (SEC), but storage time increases only from 1 h to 1.4 h while at high para concentration the same 12% increase from 83% to 95% is 3–32% more energy intensive (depending on the conversion approach) but increases the loss-less storage time from 20 h to over a week (173 h). Therefore, it appears important to find the optimum trade-off between production energy costs and the magnitude of boil-off during adiabatic storage to determine whether the achievable storage time justifies the SEC of the LH_2 product.

A concept of dormancy related to the evaporative losses in cryogenic pressure vessels was introduced by Aceves *et al.*[112] They related the energy absorption capacity of a vessel (with a pre-set maximal vent pressure) to the rate of heat transfer from the environment. The dormancy (period of inactivity before a vessel releases H_2 to reduce pressure build up) is an important parameter for cryogenic storage acceptability. Cryogenic pressure vessels were shown to solve the problems typically associated with LH_2 tanks: evaporative losses after a short period of inactivity, or during short daily driving distances. The cumulative thermal energy absorbed while a car is parked can be calculated by multiplying the amount of hydrogen in the vessel by the total change in its specific internal energy. Dormancy is then equal to the heat absorbed divided by the environmental heat transfer rate. Once the vehicle is parked, heat transfer warms the H_2 increasing both its temperature and pressure. Dormancy ends when the pressure reaches the maximum working pressure when venting hydrogen or driving the vehicle becomes necessary to maintain pressure within the vessel rating. Moreover para–ortho conversion extends dormancy because during conversion to the ortho variety, as it warms up, hydrogen absorbs considerable thermal energy (700 kJ kg^{-1}). Cryogenic pressure vessels' reduced sensitivity to environmental heat transfer was demonstrated by the typical containment of hydrogen with no evaporative losses for 8.5 days with a 4.5 Watt heat transfer rate.

I introduced a concept of break-even time for short term hydrogen storage, defined by the period τ during which the stored hydrogen is evacuated towards the fuel cell. When expressed in hours, the energy period τ was shown to vary inversely proportional to the thermal transfer coefficient h, which is a function of the envelope wall components of the tank (expressed in W m^{-2} K^{-1}):[32]

$$\tau = \frac{1}{C \cdot h}$$

C is proportional to the surface/mass ratio (the product of the surface/volume ratio of the tank and the volumetric target – hydrogen mass to tank volume). The vessel dormancy corresponds to the planned end-use of the stored energy relative to the daily duration of each particular transportation cycle. If, for example, h = 4 W m^{-2} K^{-1}, the reservoir would dispense the stored hydrogen for $\tau_h \cong 13$ h, approximately. For a fixed thermal transfer coefficient of the external envelope, the number and the nature of the porous plug materials determine the energy period.

5. Hydrogen catalysis, research and innovation

The following concluding comments are intended to summarize some open questions raised by the catalyzed conversion of molecular hydrogen, combine the knowledge gathered across different disciplines and to consider future developments, in industrial applications, experimental measurements and finally in the theoretical concepts.

5.1 Industrial applications

The importance of the catalytic processes in the liquefaction procedures and storage of hydrogen is now recognized. A significant energy expenditure in liquefaction arises from the exothermic conversion of the ortho-hydrogen isomer into the para-hydrogen form.[30] One of the key challenges in

hydrogen liquefaction plants is to combine the heat exchange and converter units. The present tendency is to insert the catalyst into plate fin thermal exchangers that accommodate direct (and recycling counter) currents. Continuous ortho-to-para conversion in commercial hydrogen plants has been promoted since the reversible process consumes less additional work and avoids excessive amounts of boil-off gas. However partial conversion might be sufficient for practical use of hydrogen energy, particularly when that energy is rapidly transformed into electrical or chemical energies.

Several research efforts focused on improving ortho–para conversion efficiencies have been reported. Comparing the ''Oxisorb'' and ''Ionex'' adsorption patterns, hydrogen on Cr-doped silica is less tightly bound than on ferric oxide gel. It is therefore easier to adsorb and desorb and the mobility on the surface is greater. Hydrogen is strongly bound to the very polar ferric oxide surface as well as to the oxygen ions, and is not disturbed by the increasing amount of hydrogen present.[61] Consequently the conversion seems to be favored both by the electronegativity of the surface and by the decrease in o–p energy due to its hindered rotation (up to about half of its free value) leading to satisfactory performance in the present liquefiers, but less for hydrogen storage since the surface of the ferric oxide gel saturates at loadings of about half a monolayer. However, further investigations are necessary since the catalyst porosity and magnetism were found to decrease as a function of time and a pronounced drop was observed in the efficiency of the ferric hydroxide gels, after prolonged use.[61] Alternative catalyst materials have been found to improve the catalytic activity of iron oxide and reduce the cooling power consumption of the heat exchanger. For example, nickel ions or nickel oxide inserted inside a silica or a MOF-74 support catalyst have shown increased efficiencies.[66,67,97] The use of Ionex catalysts for industrial purposes dates back to the late sixties and a new generation is desired to coordinate the surface magneto-chemical properties with the mesoporous structure and the thermal conductivity of the catalyst.

Nearly all present LH_2 storage vessels imply excessive mechanical containment and intensive thermal insulation,[110] resulting in significant investments in their manufacture, production and maintenance. I suggested an alternative ''short term'' hydrogen storage using a barrage system of successive microporous catalysts cumulating multiple functions: mechanical, thermal, adsorbing and catalytic. That barrage-system stabilizes the flow, delays the temperature increase by the conversion of para molecules in ortho spinning ones (a process opposite to that occurring in liquefiers). The pressure increase is limited to about 150 bar through successive JT expansions. In this kind of device, the catalysts are inserted within multiple-embedded containers between which the hydrogen gas flows, as continuous currents and countercurrents feeding a fuel cell. The incoming thermal heat which initiates liquid evaporation is transformed into a directional hydrogen flow. The microporous catalysts could be structured from activated carbons, pyrolyzed graphite, or zeolites with embedded ionic fragments. They exhibit a variety of diffusive patterns through their labyrinthine frameworks, revealing important capacities for simultaneously increasing storage capabilities, enabling pressure expansion and acting as efficient catalysts.

5.2 Experimental investigations

Without any doubt, the major advance in the experimental measurements of the ortho and para nuclear-spin isomers is provided by the ''*in situ*'' and ''site-specific'' Raman or infra-red spectra.[36] The relaxation of isomers towards thermal proportions can now be followed in real-time. For hydrogen mixtures enriched in various ortho concentrations, o- and p-lines are clearly identified from their dynamical and simultaneous ''*in situ*'' o-decrease and p-increase. ''Site-specific'' infra-red measurements were carried out for hydrogen physisorbed in the pores of metal–organic frameworks (MOF), by varying the amount of adsorbed hydrogen, exploring and comparing the IR lines corresponding to molecules adsorbed on different metal, oxygen or organic sites.[20] In particular, a striking and previously underestimated observation was that the contribution of the oxygen ions to the conversion rates was found to be almost similar to that of the metallic ones. Raman spectroscopy is now able to analyze the conversion process of the hydrogen molecules in nanocages, by following the progressive loading of the molecules on the various sites. As the temperature was decreased by cooling from 77 to 20 K, the ortho–para patterns could be correlated to the charge density measurements in the pores considered as electric nanocages in which the H_2 molecules are physically trapped.[94] Consequently the electronic structures of the catalysts' surfaces have become as strategic as their magnetic properties.[52,117]

Dynamical conversion measurements are also new and fruitful. In a recent experiment, kinetic data were acquired by using *in situ* Raman spectroscopy *via* a fiber optic cable. The ortho–para composition was recorded as a function of hydrogen flow space velocity through a hydrous ferric oxide catalyst, at a controlled temperature of 77 K, in order to test various kinetic models.[72,96]

The development of combining new radiative measurements (IR, Raman, and REMPI) with other surface spectroscopy techniques such as X-rays or neutron beams,[60,61] thermal- or photo-induced desorption[50] allows the correlation of nuclear-spin populations with structural changes in the H_2 arrangement on catalytic surfaces.

In 2021, Barnett *et al.*[80,81] investigated mechanisms of chemisorption at open metal sites within porous frameworks and in particular showed that non-dissociative chemisorption of H_2 at the trigonal pyramidal Cu^+ sites in a metal–organic framework occurs *via* a metastable physisorbed precursor species. Evidence for this precursor intermediate was also provided by temperature-programmed desorption and density functional theory calculations. The activation barrier separating the precursor species from the chemisorbed state was shown to correlate with a change in the Cu^+ coordination environment that enhances π-backbonding with H_2. Ultimately, these findings demonstrated that adsorption at framework metal sites does not always follow a concerted pathway and

underscores the importance of probing kinetics in the design of next-generation adsorbents. Physisorbed precursors might become relevant intermediates in catalytic processes within porous solids.

As reviewed in the present study, numerous porous materials exhibiting a variety of diffusive patterns through their labyrinthic frames have revealed significant capabilities in simultaneously performing thermal and pressure expansion as well as catalytic activity. Simple activated carbons, pyrolyzed graphite, or even zeolites with embedded ionic fragments would be sufficient for the vessel prototypes intended for immediate applications. More complex catalytic plugs with increased storage capabilities should be analyzed further for flow regulation and gate functions in a second stage.

5.3 Theoretical interpretations and progress

Any sample of molecular hydrogen is a compound of two nuclear spin varieties: the ortho and para ones. When the sample is in thermal equilibrium with a thermostat, it behaves as a single gas. But if not, it behaves as a mixture of two different varieties. Tendencies towards separate equilibria compete with a global one. In most applications the hydrogen flow is not in thermal equilibrium with the environment or with a catalyst if any, and is subjected to complex irreversible processes.

The discovery that catalyst electrons are able to convert the hydrogen spin isomers *via* Coulomb repulsion has enlarged the field of conversion research.[45,46] For a century, the conversion catalytic process was exclusively attributed to a magnetic mechanism, as induced by the local magnetic moments of the catalyst surface. This kind of dipolar interaction is very short-ranged; the molecule must approach at less than say 3 Å of the magnetic site and remain there for a while to be converted. In contrast, the Coulomb interaction has a longer range, necessitating some overlap between the catalyst and molecular electron clouds. This mechanism combines a virtual electron excitation with a magnetic one, although the magnetic step is internal to the molecule. Altogether, this kind of electromagnetic process can combine various channels and dynamics. The first one that Sugano and I introduced was the XY exchange–contact one (electron exchanges followed by internal electron–nucleus contact), which was intended to interpret the disparity in conversion rates over magnetic chromia–alumina catalysts.[45] A few years later I interpreted the IBM observation of conversion over non-magnetic noble metals, through a charge transfer mechanism (also combined with a contact step) denoted as UY, in which the molecular o–p energy and momentum were dissipated by the emission of electron–hole pairs through the conduction band.[46,47] During the last decade, after the experimental confirmation of my model of the silver catalyzed conversion, I interpreted a variety of new conversion measurements over insulating or semiconductor catalysts, MOF-74,[51–53] Si,[54] and ASW[55] by introducing an additional spin–orbit coupling of the catalyst electrons leading to the USY and XSY channels.

Considering the dynamical side of the conversion patterns, I was led to consider a variety of collective processes: magnons, phonons, electron hole pairs or triplet excitons. The catalytic process is no longer restricted to a local or surface effect but has been extended to the full range of degrees of freedom of the solid bulk. On the molecular side the conversion process is no longer restricted to the ground rotational states but also involves the full spectrum of unoccupied excited states, vibrational or electronic. High electronic transitions induced by long range electron fluctuations can be shared by multiple adsorbed molecules, and such processes should be examined in more detail in the future. The analysis of the catalytic reactions involving hydrogen mixtures has therefore come closer to the electromagnetic processes at play in chemical reactions.

Considering the magnetic characteristics of efficient catalysts and their effects on the conversion process, I have interpreted their efficiencies in terms of the ability of catalyst magnons to dissipate the o–p energy.[42,43] Recent experimental studies have shown that the ferric oxide gel contains pair–pair correlations up to approximately 3 nm. The first three positive correlations can be ascribed to Fe–O, O–O, and Fe–Fe pairs.[61] Such correlations can accommodate the spin fluctuations emitted by the hydrogen conversion. Although not ferromagnetic on a macroscopic scale the ferric oxide gel has a large capacity to adsorb o–p energy and redistribute it among dozens of spin pairs for each adsorbed molecule. Such excitations might be described as para-magnons of intermediate range.

Progress in the development of new catalysts for industrial applications will depend on adapting each of them to a specific function, temperature and pressure range, while integrating the results obtained from experimental measurements and their theoretical interpretations. It would also be beneficial to incorporate the results obtained from more advanced disciplines, such as chemically induced magnetic polarization (CIDNP)[114] and para-hydrogen-induced polarization (PHIP) methods,[115,116] which are are powerful techniques for studying hydrogen polarization transfers and more generally the magneto-optics phenomena.[117]

Conflicts of interest

There are no conflicts to declare.

Data availability

My review does not contain research data as digital, machine-readable files.

References

1 S. Tomonaga, *The story of spin*, The University of Chicago Press, 1977.
2 D. M. Dennison, A note on the Specific Heat of the Hydrogen Molecule, *Proc. R. Soc. London, Ser. A*, 1927, **A115**, 483–486 Recollections of Physics and Physicists during the 1920's, 1974, Ann. J. Phys. 42.1051-6.

3 E. P. Wigner, Über die paramagnetische Umwandlung von Para–Ortho wasserstoff. III, *Part I Phys. Chem. Part II Solid State Phys.*, 1997, **23**, 126–130, DOI: 10.1007/978-3-642-59033-7_11.
4 D. H. Weitzel, C. Van Valin and J. W. Draper, *Advances in Cryogenic Engineering*, Springer, 1960, pp. 73–84, DOI: 10.1007/978-1-4684-3105-6_.
5 D. H. Weitzel, *J. Res. Nat. Bur. Stand.*, 1958, **A60**, 2840.
6 N. Wakao, J. M. Smith and P. W. Selwood, *J. Catal.*, 1962, **1**, 62–73.
7 P. W. Selwood, *J. Am. Chem. Soc.*, 1965, **87**, 1804.
8 P. W. Selwood, *Adv. Catal.*, 1978, **27**, 23.
9 M. Misono and P. W. Selwood, *J. Am. Chem. Soc.*, 1968, **90**, 2977.
10 M. Misono and P. W. Selwood, *J. Am. Chem. Soc.*, 1969, **91**, 1300.
11 C. F. Ng and P. W. Selwood, Magnetic effects on the ortho–para hydrogen conversion over α-Cr_2O_3, CoO, and MnO, *J. Catal.*, 1976, **43**, 252.
12 P. W. Selwood, Extrinsic field conversion of parahydrogen over the rare earths, *J. Catal.*, 1970, **19**, 353–359, DOI: 10.1016/0021-9517(70)90258-7.
13 P. W. Selwood, *Nature*, 1970, **228**, 278.
14 P. Avouris, D. Schmeisser and J. E. Demuth, Observation of Rotational Excitations of hydrogen adsorbed on Ag surfaces, *Phys. Rev. Lett.*, 1982, **48**, 199.
15 S. Andersson and J. Harris, Observation of Rotational Transitions for H_2, D_2 and HD Adsorbed on Cu(100), *Phys. Rev. Lett.*, 1982, **48**, 545.
16 R. E. Palmer and R. F. Willis, Rotational States of Physisorbed Hydrogen on Graphite, *Surf. Sci.*, 1987, **179**, L1.
17 E. V. Lavrov and J. Weber, Ortho and Para Interstitial H_2 in Silicon, *Phys. Rev. Lett.*, 2002, **89**, 215501.
18 M. Hiller, E. V. Lavrov and J. Weber, Ortho–Para Conversion of Interstitial in Si, *Phys. Rev. Lett.*, 2007, **98**, 055504.
19 C. Peng, M. Stavola, W. B. Fowler and M. Lockwood, Ortho–para transition of interstitial H_2 and D_2 in Si., *Phys. Rev.*, 2009, **B80**, 125207.
20 S. A. FitzGerald, J. Hopkins, B. Burkholder, M. Friedman and J. L. C. Rowsell, Quantum dynamics of adsorbed normal- and para-H_2, HD, and D_2 in the microporous framework MOF-74 analyzed using infrared spectroscopy, *Phys. Rev. B: Condens. Matter Mater. Phys.*, 2010, **81**, 104305, DOI: 10.1103/physrevb.81.104305.
21 H. Ueta, N. Watanabe, T. Hama and A. Kouchi, Surface Temperature Dependence of Hydrogen Ortho–Para Conversion on Amorphous Solid Water, *Phys. Rev. Lett.*, 2016, **116**, 253201, DOI: 10.1103/physrevlett.116.253201.
22 K. Yamakawa and K. Fukutani, Nuclear Spin Conversion of H_2, H_2O, and CH_4 Interacting with Diamagnetic Insulators, *J. Phys. Soc. Jpn.*, 2020, **89**, 051016–051028, DOI: 10.7566/jpsj.89.051016.
23 X. Zhang, T. Karman, G. C. Groenenboom and A. Van der Avoird, Para–ortho hydrogen conversion: Solving a 90-year old mystery, *Nat. Sci.*, 2021, 1–8, DOI: 10.1002/ntls.10002.
24 B. Friedrich, A paramount problem solved at last: Paramagnetic Catalysis of op hydrogen conversion, *Nat. Sci.*, 2021, e10004, DOI: 10.1002/ntls.10004.
25 D. H. Weitzel, W. V. Loebenstein, J. W. Draper and O. E. Park, Ortho–Para Catalysis In Liquid-Hydrogen Production, *J. Res. Natl. Bur. Stand.*, 1958, **A60**, 221.
26 P. L. Barrick, L. F. Brown, H. L. Hutchinson and R. L. Cruse, Improved Ferric oxyde gel catalysts for ortho–para hydrogen conversion, *Adv. Cryog. Eng.*, 1964, **10**, D1.
27 H. L. Hutchinson, P. L. Barrick and L. F. Brown, *in Advances in Cryogenic Engineering*, Springer US, Boston, MA, 1965, pp. 190–196.
28 B. da Silva Falcão, K. Jeong, S. Al Ghafri, N. Robinson, L. Tang, K. Kozielski and M. L. Johns, Ortho- to para-hydrogen catalytic conversion kinetics, *Int. J. Hydrogen Energy*, 2024, **62**, 345–351.
29 M. S. Lipman, H. Cheung and O. P. Roberts, Continuous conversion hydrogen liquefaction, *CEP*, 1963, **59**, 49.
30 P. V. Mendoza-Moreno, G. J. Fulham and E. J. Marek, Harnessing the enigmatic ortho–para isomeric conversion for energy-efficient and low-carbon production of liquid hydrogen, *Cell Rep. Sustainability*, 2024, **1**, 100243.
31 C. R. Baker and R. L. Shaner, A study of the efficiency of hydrogen liquefaction, *Int. J. Hydrogen Energy*, 1978, **3**, 321–334.
32 E. Ilisca, Hydrogen Storage in Cryogenic, Cybernetic, and Catalytic Vessels for Transport Vehicles, *J. Energy Power Technol.*, 2021, **3**(4), 45.
33 A. Farkas, *Orthohydrogen, Parahydrogen and Heavy Hydrogen*, Cambridge University Press, Cambridge, UK, 1935.
34 E. Ilisca, Ortho–Para Conversion of Hydrogen on Surfaces, *Prog. Surf. Sci.*, 1992, **41**, 213–336.
35 E. Ilisca and A. P. Legrand, Theoretical rates and correlation functions in o–p hydrogen conversion on paramagnetic surfaces, *Phys. Rev.*, 1972, **B5**, 4994.
36 E. Ilisca, Hydrogen conversion in nanocages, *Hydrogen*, 2021, **2**, 160–206, DOI: 10.3390/hydrogen2020010.
37 L. G. Harrison and C. A. Mc Dowell, *Proc. R. Soc. London, Ser. A*, 1953, **A220**, 77.
38 K. Makoshi and E. Ilisca, Dipolar and contact processes in H_2 o–p conversion on ionic surfaces, *J. Phys.: Condens. Matter*, 1993, **5**, 7325.
39 E. Ilisca and S. Paris, Magnetic Field Acceleration of the o–p H_2 conversion on Transition Oxides, *Phys. Rev. Lett.*, 1999, **82**, 1788.
40 R. E. Svadlenak and A. B. Scott, The Conversion of Ortho to Parahydrogen on Iron Oxide–Zinc Oxide Catalysts, *J. Am. Chem. Soc.*, 1957, **79**, 5385.
41 R. A. Buyanov, Hydrogen conversion on transition oxides, *Kinetica i Kataliz*, 1980, **1**, 306418, 617.
42 E. Ilisca, Theoretical calculation of a new effect in ortho–para H_2 conversion on magnetic surfaces, *Phys. Rev. Lett.*, 1970, **24**, 797.
43 E. Ilisca, Experimental evidence for a new effect in ortho–para H_2 conversion on magnetic surfaces, *Phys. Lett.*, 1970, **33A**, 247.
44 R. Muhida, H. Setiyanto, M. Rahman Md, W. A. Dino, H. Nakanishi, H. Kasai, K. Fukutani and T. Okano, Ortho–para H_2 conversion on multiple-decked sandwich clusters

of $M(C_6H_6)_2$ (M = Mn, Fe, Co) induced by an inhomogeneity of spin density distribution, *Thin Solid Films*, 2006, 509223–509226.

45 E. Ilisca and S. Sugano, A new channel in ortho–para H_2 conversio, *Phys. Rev. Lett.*, 1986, **57**, 2790.

46 E. Ilisca, Ortho–para H_2 conversion on a cold Ag(111) metal surface, *Phys. Rev. Lett.*, 1991, **66**, 667–670, DOI: **10.1103/physrevlett.66.667**.

47 E. Ilisca, Ortho–para hydrogen conversion on noble metals, *J. Phys. I*, 1991, **1**, 1785–1807.

48 K. Fukutani, K. Yoshida, M. Wilde, W. A. Diño, M. Matsumoto and T. Okano, Photostimulated Desorption and Ortho–Para Conversion of H_2 on Ag Surfaces, *Phys. Rev. Lett.*, 2003, **90**, 096103, DOI: **10.1103/physrevlett.90.096103**.

49 K. Niki, T. Kawauchi, M. Matsumoto, K. Fukutani and T. Okano, Mechanism of Ortho–Para H_2 Conversion on Ag surfaces, *Phys. Rev.*, 2008, **B77**, 201404.

50 K. Fukutani and T. Sugimoto, Ortho–Para Conversion of Molecular Hydrogen in Physisorption States on Solid Surfaces, *Prog. Surf. Sci.*, 2013, **88**, 279.

51 E. Ilisca, Hydrogen conversion on non-magnetic insulating surfaces, *Europhys. Lett.*, 2013, **104**, 18001, DOI: **10.1209/0295-5075/104/18001**.

52 E. Ilisca and F. Ghiglieno, Electron exchanges in nuclear spin conversion of hydrogen physisorbed on diamagnetic insulators, *Eur. Phys. J. B*, 2014, **87**, 235–264, DOI: **10.1140/epjb/e2014-50282-2**.

53 E. Ilisca and F. Ghiglieno, Nuclear conversion theory: molecular hydrogen in non-magnetic insulators, *R. Soc. Open Sci.*, 2016, **3**, 160042, DOI: **10.1098/rsos.160042**.

54 E. Ilisca and F. Ghiglieno, Electronuclear paths in the nuclear conversion of molecular hydrogen in silicon, *Chem. Phys. Lett.*, 2017, **667**, 233–237, DOI: **10.1016/j.cplett.2016.11.056**.

55 E. Ilisca, Electromagnetic nuclear spin conversion: Hydrogen on amorphous solid water, *Chem. Phys. Lett.*, 2018, **713**, 289–292, DOI: **10.1016/j.cplett.2018.10.053**.

56 M. Fujiwara, K. Niki, T. Okano and K. Fukutani, Ortho–para conversion of hydrogen molecules on Cr_2O_3(0001)/Cr(110) surfaces, *J. Phys.: Conf. Ser.*, 2010, **200**, 22038, DOI: **10.1088/1742-6596/200/2/022038**.

57 H. Ueta and K. Fukutani, Rotational-energy transfer in H_2 ortho–para conversion on a metal surface: Interplay between electron and phonon systems, *J. Phys. Chem. Lett.*, 2023, **14**(34), 7591–7596, DOI: **10.1021/acs.jpclett.3c01209**.

58 H. Ueta, K. Fukutani and K. Yamakawa, Fast ortho to para conversion of molecular hydrogen in chemisorption and matrix-isolation systems, *Front. Chem.*, 2023, **11**, 1258035, DOI: **10.3389/fchem.2023.1258035**.

59 H. Ueta, N. Watanabe, T. Hama and A. Kouchi, Surface Temperature Dependence of Hydrogen Ortho–Para Conversion on on Amorphous Solid Water, *Phys. Rev. Lett.*, 2016, **116**, 253201, DOI: **10.1103/PhysRevLett.116.253201**.

60 G. Romanelli, S. Rudić, M. Zanettia, C. Andreani, F. Fernandez-Alonsoa, G. Gorinic, M. Krzystyniak and G. Škoro, Measurement of the para-hydrogen concentration in the ISIS moderators using neutron transmission and thermal conductivity, *Nucl. Instrum. Methods Phys. Res., Sect. A*, 2018, **888**, 88–95, DOI: **10.1016/j.nima.2018.01.039**.

61 M. Hartl, R. Chad Gillis, L. Daemen, D. P. Olds, K. Page, S. Carlson, Y. Cheng, T. Hugle, E. B. Iverson, A. J. Ramirez-Cuesta, Y. Lee and G. Muhrera, Hydrogen adsorption on two catalysts for the ortho- to parahydrogen conversion: Cr-doped silica and ferric oxide gel, *Phys. Chem. Chem. Phys.*, 2016, **18**, 17281, DOI: **10.1039/c6cp01154c**.

62 D. H. Weitzel, J. H. Blake and M. Konecnik, *Adv. Cryog. Eng.*, 1960, **4**, 286–295, DOI: **10.1007/978-1-4757-0540-925**.

63 T. Das, S. C. Kweon, I. W. Nah, S. W. Karng, J. G. Choi and I. H. Oh, Spin conversion of hydrogen using supported iron catalysts at cryogenic temperature, *Cryogenics*, 2015, **69**, 36–43.

64 J. H. Kim, S. W. Karng, I. H. Oh and I. W. Nah, Ortho-para hydrogen conversion characteristics of amorphous and mesoporous Cr_2O_3 powders at a temperature of 77 K, *Int. J. Hydrogen Energy*, 2015, **40**, 14147–14153.

65 J. H. Kim, S. W. Kang, I. W. Nah and I. H. Oh, Synthesis and characterization of Fe-modified zeolite for spin conversion of hydrogen at cryogenic temperature, *Int. J. Hydrogen Energy*, 2015, **40**, 15529–15533.

66 S. A. FitzGerald, B. Burkholder, M. Friedman, J. B. Hopkins, C. J. Pierce and J. M. Schloss, Metal-specific interactions of H_2 adsorbed within isostructural metal organic frameworks, *J. Am. Chem. Soc.*, 2011, **133**, 20310–20318.

67 Y. Si, W. Wang, E. M. El-Sayed and D. Yuan, Use of breakthrough experiment to evaluate the performance of hydrogen isotope separation for metal–organic frameworks M-MOF-74 (M = Co, Ni, Mg, Zn), *Sci. China: Chem.*, 2020, **63**, 881–889.

68 D. M. Polyukhov, N. A. Kudriavykh, S. A. Gromilov, A. S. Kiryutin, A. S. Poryvaev and M. V. Fedin, *ACS Energy Lett.*, 2022, **7**, 4336–4341.

69 N. A. Zubir, C. Yacou, J. Motuzas, X. Zhang and J. C. da Costa, Structural and functional investigation of graphene oxide-Fe_3O_4 nanocomposites for the heterogeneous Fenton-like reaction, *Sci. Rep.*, 2014, **4**, 1–8.

70 A. H. Singleton, A. Lapin and L. A. Wenzel, *Adv. Cryog. Eng.*, 1968, **13**, 409–427.

71 S. Al Ghafri, S. Munro, U. Cardella, T. Funke, W. Notardonato, J. P. Martin Trusler, J. Leachman, R. Span, S. Kamiya, G. Pearce, A. Swanger, E. D. Rodriguez, P. Bajada, F. Jiao, K. Peng, S. Arman, M. L. Johns and E. F. May, Hydrogen liquefaction: a review of the fundamental physics, engineering practice and future opportunities, *Energy Environ. Sci.*, 2022, **15**, 269.

72 F. Jiao, S. Al Ghafri, K. T. O'Neill, P. S. Stanwix, G. M. Sellner, E. O. Fridjonsson, N. Robinson, E. F. May and M. L. Johns, Review of hydrogen ortho–para conversion: Experimental data and reaction kinetics, Reaction Chemistry & Engineering, *Spec. Publ. – R. Soc. Chem.*, 2024, **9**, 2846–2862.

73 T. Das, J. G. Choi and I. H. Oh, Synthesis of Highly Effective α-Fe_2O_3 Catalyst for the Spin Conversion of Liquid Hydrogen, *Proc. Natl. Acad. Sci., India, Sect. A*, 2020, **90**, 399–409, DOI: **10.1007/s40010-019-00599-3**.
74 N. J. Turro, J. Y.-C. Chen, E. Sartori, M. Ruzzi, A. Marti, R. Lawler, S. Jockusch, J. Lopez-Gejo, K. Komatsu and Y. Murata, The Spin Chemistry and Magnetic Resonance of H_2@C_{60}. From the Pauli Principle to Trapping a Long Lived Nuclear Excited Spin State inside a Buckyball, *Acc. Chem. Res.*, 2010, **43**, 335–345, DOI: **10.1021/ar900223d**.
75 H. K. Chae, D. Y. Siberio-Perez, J. Kim, Y. Go, M. Eddaoudi, A. J. Matzger, M. O'Keeffe and O. M. Yaghi, A route to high surface area, porosity and inclusion of large molecules in crystals, *Nature*, 2004, **427**, 523.
76 J. L. Rowsell, A. R. Millward, K. S. Park and O. M. Yaghi, Hydrogen sorption in functionalized metal–organic frameworks, *J. Am. Chem. Soc.*, 2004, **126**, 5666–5667.
77 J. L. Rowsell and O. M. Yaghi, Strategies for hydrogen storage in metal–organic frameworks, *Angew. Chem., Int. Ed.*, 2005, **44**, 4670–4679.
78 M. Eddaoudi, J. Kim, N. Rosi, D. Vodak, J. Wachter and M. O'Keeffe, *et al.*, Systematic design of pore size and functionality in isoreticular MOFs and their application in methane storage, *Science*, 2002, **295**, 469–472.
79 P. M. Forster, J. Eckert, J.-S. Chang, S.-E. Park, G. F. Srey and A. K. Cheetham, Hydrogen Adsorption in Nanoporous Nickel(II) Phosphates, *J. Am. Chem. Soc.*, 2003, **125**, 1309.
80 B. R. Barnett, H. A. Evans, G. M. Su, H. Z. H. Jiang, R. Chakraborty, D. Banyeretse, T. J. Hartman, M. B. Martinez, B. A. Trump, J. D. Tarver, M. N. Dods, L. M. Funke, J. Börgel, J. A. Reimer, W. S. Drisdell, K. E. Hurst, T. Gennett, S. A. FitzGerald, C. M. Brown, M. Head-Gordon and J. R. Long, Observation of an Intermediate to H_2 Binding in a Metal−Organic Framework, *J. Am. Chem. Soc.*, 2021, **143**, 14884–14894.
81 R. Chakraborty, J. J. Talbot, H. Shen, Y. Yabuuchi, K. M. Carsch, H. Z. Jiang, H. H. Furukawa, J. R. Long and M. Head-Gordon, Quantum chemical modeling of hydrogen binding in metal–organic frameworks, *Phys. Chem. Chem. Phys.*, 2024, **26**, 6490–6511.
82 C. M. Cunningham and H. L. Johnston, *J. Am. Chem. Soc.*, 1958, **80**, 2377.
83 D. S. Chapin, C. M. Cunningham and H. L. Johnston, *J. Am. Chem. Soc.*, 1958, **80**, 2382.
84 E. Poirier, R. Chahine and T. K. Bose, Hydrogen adsorption in carbon nanostructures, *Int. J. Hydrogen Energy*, 2001, **26**, 831–835.
85 P. Bénard and R. Chahine, Modeling of adsorption storage of hydrogen on activated carbons, *Int. J. Hydrogen Energy*, 2001, **26**, 849–855.
86 M. A. Richard, P. Bénard and R. Chahine, Gas adsorption process in activated carbon over a wide temperature range above the critical point. Part 1: Modified Dubinin–Astakhov model, *Adsorption*, 2009, **15**, 43–51.
87 R. Paggiaro, W. Polifke and P. Bénard, Cryo-adsorptive hydrogen storage on activated carbon. I: Thermodynamic analysis of adsorption vessels and comparison with liquid and compressed gas hydrogen storage systems, *Int. J. Hydrogen Energy*, 2010, **35**, 638–647.
88 Q. Wang and J. K. Johnson, Molecular simulation of hydrogen adsorption in single-walled carbon nanotubes and idealized carbon slit pores, *J. Chem. Phys.*, 1999, **110**, 577.
89 H. L. Hutchinson, L. F. Brown and P. L. Barrick, in *Advances in Cryogenic Engineering: Proceeding of the 1970 Cryogenic Engineering Conference*, ed. D. Timmerhaus, The University of Colorado, Boulder, Colorado, Springer US, Boston, MA, 1971, pp. 96–103, DOI: **10.1007/978-1-4757-0244-6_12**.
90 Ø. Wilhelmsen, D. Berstad, A. Aasen, P. Nekså and G. Skaugen, Reducing the exergy destruction in the cryogenic heat exchangers of hydrogen liquefaction processes, *Int. J. Hydrogen Energy*, 2018, **43**, 5033–5047.
91 T. Das, J. G. Cho and I. H. Oh, Synthesis of Highly Effective α-Fe_2O_3 Catalyst for the Spin Conversion of Liquid Hydrogen, *Proc. Natl. Acad. Sci., India, Sect. A*, 2020, **90**, 399–409, DOI: **10.1007/s40010-019-00599-3**.
92 W. E. Carlos and P. C. Taylor, Molecular hydrogen in a-Si, *Phys. Rev. B: Condens. Matter Mater. Phys.*, 1982, **25**, 1435.
93 E. E. Chen, M. Stavola, W. B. Fowler and P. Walters, Key to Understanding Interstitial H_2 in Si, *Phys. Rev. Lett.*, 2002, **88**, 105507.
94 T. Kosone, A. Hori, E. Nishibori, Y. Kubota, A. Mishima, M. Ohba, H. Tanaka, K. Kato, J. Kim and J. A. Real, Coordination nano-space as stage of hydrogen ortho–para conversion, *R. Soc. Open Sci.*, 2015, **2**, 150006, DOI: **10.1098/rsos.150006**.
95 G. E. Schmauch and A. H. Singleton, Technical Aspects of Ortho–Para hydrogen Conversion, *Ind. Eng. Chem.*, 1964, **56**, 20–31, DOI: **10.1021/ie50653a003**.
96 G. Valenti, in *Compendium of Hydrogen Energy: Hydrogen Storage, Distribution and Infrastructure*, ed. R. Gupta, A. Basile and T. Nejat Veziroglu, Woodhead Publishing, Cambridge, 2016, vol. 2.
97 A. V. Zhuzhgov, O. P. Krivoruchko, L. A. Isupova, O. N. Mart'yanov and V. N. Parmon, Low-Temperature Conversion of ortho-Hydrogen into Liquid para-Hydrogen: Process and Catalysts, *Catal. Ind.*, 2018, **10**(1), 9–19, DOI: **10.1134/S2070050418010117**.
98 J. J. Teng, K. Wang, S. L. Zhu, S. R. Bao, X. Q. Zhi, X. B. Zhang and L. M. Qiu, Comparative study on thermodynamic performance of hydrogen liquefaction processes with various ortho–para hydrogen conversion methods, *Energy*, 2023, **271**, 127016.
99 J. Karlsson, Master thesis, Lund University, 2017.
100 S. Fang, S. Zhu, X. Wei, J. Teng, S. Cao, K. Wang and L. Qiu, Dimensionless performance mapping of cryogenic plate-fin heat exchangers with ortho–para hydrogen continuous conversion for hydrogen liquefaction, *Energy*, 2024, **313**, 133951, DOI: **10.1016/j.energy.2024.133951**.
101 L. Tang, D. Yamaguchi, J. Orellana and W. Tian, Multi-physics Studies of 3D Plate Fin Heat Exchanger Filled with

Ortho–Para-Hydrogen Conversion Catalyst for Hydrogen Liquefaction, *Hydrogen*, 2024, **5**, 682–709, DOI: 10.3390/hydrogen5040036.

102 K. T. O'Neill, S. Al Ghafri, B. da Silva Falcao, L. G. Tang, K. Kozielski and M. L. Johns, Hydrogen ortho–para conversion: Process sensitivities and optimization, *Chem. Eng. Process.*, 2023, **184**, 109272.

103 P. Xu, G. Lei, Y. Y. Xu, J. Wen, S. M. Wang and Y. Z. Li, Study on continuous cooling process coupled with ortho–para hydrogen conversion in plate-fin heat exchanger filled with catalyst, *Int. J. Hydrogen Energy*, 2022, **47**, 4690–4703.

104 J. Park, H. Lim, G. H. Rhee and S. W. Karng, *Int. J. Heat Mass Transfer*, 2021, **170**, 121007.

105 P. J. Donaubauer, U. Cardella, L. Decker and H. Klein, Kinetics and Heat Exchanger Design for Catalytic Ortho–Para Hydrogen Conversion during Liquefaction, *Chem. Eng. Technol.*, 2019, **42**(3), 1–12, DOI: 10.1002/ceat.201800345.

106 M. Klell, Storage of hydrogen in the pure form, *Handbook of hydrogen storage*. Wiley-VCH Verlag GmbH & Co. KgaA, Weinheim, Germany, 2010.

107 S. M. Aceves, F. Espinosa-Loza, E. Ledesma-Orozco, T. O. Ross, A. H. Weisberg and T. C. Brunner, High-density automotive hydrogen storage with cryogenic capable pressure vessels, *Int. J. Hydrogen Energy*, 2010, **35**, 1219–1226.

108 H. Barthélémy, Hydrogen storage and industrial prospectives, *Int. J. Hydrogen Energy*, 2012, **37**, 17364–17372.

109 G. Petitpas, P. Bénard, L. E. Klebanoff, J. Xiao and S. M. Aceves, A comparative analysis of the cryo-compression and cryo-adsorption hydrogen storage methods, *Int. J. Hydrogen Energy*, 2014, **39**, 10564–10584.

110 R. K. Ahluwalia and J. K. Peng, Automotive hydrogen storage system using cryo-adsorption on activated carbon, *Int. J. Hydrogen Energy*, 2009, **34**, 5476–5487.

111 R. K. Ahluwalia, T. Q. Hua, J.-K. Peng, S. Lasher, K. McKenney and J. Sinha, Technical assessment of cryo-compressed hydrogen storage tank systems for automotive applications, *Int. J. Hydrogen Energy*, 2010, **35**, 4171–4184.

112 R. K. Ahluwalia, T. Q. Hua and J. K. Peng, On-board and off-board performance of hydrogen storage options for light-duty vehicles, *Int. J. Hydrogen Energy*, 2012, **37**, 2891–2910.

113 S. M. Aceves, G. Petitpas, F. Espinosa-Loza, M. J. Matthews and E. Ledesma-Orozco, Safe, long range, inexpensive and rapidly refuelable hydrogen vehicles with cryogenic pressure vessels, *Int. J. Hydrogen Energy*, 2013, **38**, 2480–2489.

114 A. R. Lepley and G. L. Closs, *Chemically Induced Magnetic Polarization*, John Wiley, NY, 1973.

115 K. M. Salikhov, Y. N. Molin, R. Z. Sagdeev and A. L. Buchachenko, *Spin Polarization and Magnetic Effects in Radical Reactions*, Elsevier, Amsterdam, The Netherlands, 1984.

116 C. R. Bowers and D. P. Weitekamp, Transformation of symmetrization order to nuclear-spin magnetization by chemical reaction and nuclear magnetic resonance, *Phys. Rev. Lett.*, 1986, **57**, 2645–2648.

117 E. Ilisca, Magneto-optic and magneto-catalytic effect, *J. Magn. Soc. Jpn.*, 1987, **11**, 13.

